A crustal-scale view at rift localization along the fossil Adriatic margin of the Alpine Tethys preserved in NW Italy.

M. Beltrando, D. F. Stockli, A Decarlis, Gianreto Manatschal

AGU PUBLICATIONS

Tectonics

RESEARCH ARTICLE
10.1002/2015TC003973

Key Points:
- Heating-cooling cycles in rift systems
- Relationship between crustal-scale heating-cooling cycles and the onset of rifting
- Rift localization possibly triggered by regional-scale thermal anomaly

Supporting Information:
- Text S1

Correspondence to:
M. Beltrando,
marco.beltrando@unito.it

Citation:
Beltrando, M., D. F. Stockli, A. Decarlis, and G. Manatschal (2015), A crustal-scale view at rift localization along the fossil Adriatic margin of the Alpine Tethys preserved in NW Italy, *Tectonics*, *34*, 1927–1951, doi:10.1002/2015TC003973.

Received 15 JUL 2015
Accepted 21 AUG 2015
Accepted article online 25 AUG 2015
Published online 28 SEP 2015

A crustal-scale view at rift localization along the fossil Adriatic margin of the Alpine Tethys preserved in NW Italy

Marco Beltrando[1], Daniel F. Stockli[2], Alessandro Decarlis[3], and Gianreto Manatschal[3]

[1]Dipartimento di Scienze della Terra, Università di Torino, Torino, Italy, [2]Department of Geological Sciences, University of Texas at Austin, Austin, Texas, USA, [3]CNRS-EOST, Université de Strasbourg, Strasbourg, France

Abstract Fossil rifted margins, whereby originally extended continental crust is subsequently stacked in orogenic belts, provide the opportunity to track rift-related tectonics across different crustal levels. In this study, the tectonothermal evolution of the fossil Adriatic continental margin, sampled in the Italian Southern Alps, is investigated combining new (U-Th)/He zircon (ZHe) thermochronology from upper crustal rocks with existing data from the originally underlying lower crust, to shed light on the processes responsible for rift localization in the Alpine Tethys system. The Adriatic microplate records a protracted rift evolution, whereby distributed upper crustal stretching at 245–190 Ma was followed by rift localization along its future western edge, culminating in mantle exhumation at 165–160 Ma. A progressive westward younging of ZHe ages, from 280–240 Ma in the Lombardian Basin to 215–200 Ma near the Sostegno and Fenera Basins, indicates that anomalously high thermal gradients were established in the Late Triassic in the area where rifting later localized. The inferred episodic heating was contemporaneous with protracted fluid flow, minor magmatism, and ductile shearing within the originally underlying lower crust. Subsequent normal faulting was initiated post-185 Ma, as constrained by exhumation-related ZHe ages in detrital zircons from a syntectonic sandstone. The spatial distribution of the detected heating-cooling cycle suggests that rift localization along the western edge of the Adriatic Plate was probably favored by a crustal-scale thermal anomaly, established at 215–210 Ma, followed by thermal decay by 200–190 Ma. Subsequent crust-wide extension, starting at 185–180 Ma, led to excision of continental crust and mantle exhumation.

1. Introduction

Rifted continental margins commonly record multiple stages of diffuse crustal stretching [e.g., *Direen et al.,* 2007; *Faleide et al.,* 2008; *Ball et al.,* 2013]. Within this context, renewed stretching is not necessarily localized along domains that accommodated greater extension during the previous rifting stages [e.g., *Cowie et al.,* 2005; *Faleide et al.,* 2008; *Pereira and Alves*, 2011]. As a result, rift systems are generally observed to shift in time and space within evolving margins, ahead of strain localization leading to lithospheric breakup. Rift migration and localization have been ascribed to a variety of processes, often involving strain softening driven by localized magmatism, possibly linked to hot spot activity [*White*, 1989; *Govers and Wortel*, 1993; *Bosworth et al.,* 2005; *Torsvik et al.,* 2013; *Buiter and Torsvik*, 2014]. However, the integrated strength of thinned continental crust may also increase in response to the interplay between extension rates and magmatism, so that stretching may be localized at the edges of previously thinned and underplated crustal sections [*Kusznir and Park*, 1987; *Van Wijk and Cloetingh,* 2002; *Direen et al.,* 2007; *Manatschal et al.,* 2015].

Similarly to present-day rifted margins, multiple rifting episodes are also characteristic of the Mesozoic evolution of Southern Europe and North Africa, during the breakup of Pangea (Figure 1). In this area, Middle Triassic opening of the Meliata and Ionian Basins [e.g., *Kozur*, 1991; *Speranza et al.,* 2012] was followed by the formation of the central Atlantic and Alpine Tethys in the latest Triassic to Middle Jurassic (Figures 1a and 1b). Hyperextension within these domains was generally preceded by several rift events displaying a complex spatial pattern [*Manatschal*, 2004]: widespread Late Triassic normal faulting in the Atlantic and Alpine Tethys rift systems, recorded in the Adriatic Plate [*Bertotti et al.,* 1993; *Gaetani*, 2010], Iberian Plate [*Pereira and Alves*, 2011], and North Africa [*Gouiza et al.,* 2010], led to the formation of wide basins characterized by relatively low stretching factors, prior to localization of extension within a narrow corridor, eventually culminating in crustal separation (Figure 1b).

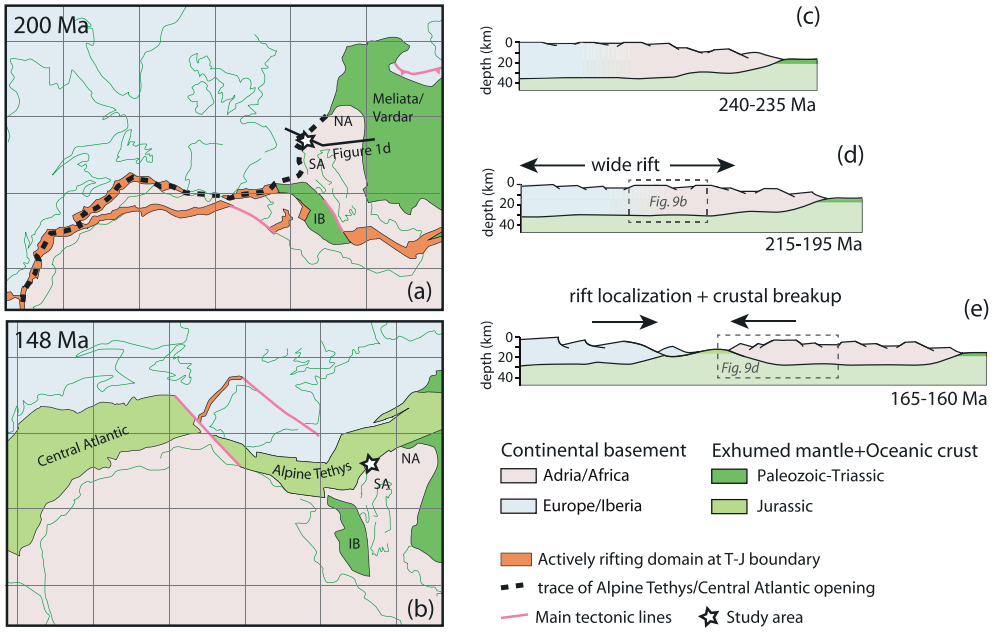

Figure 1. Paleogeographic reconstruction of the Northern Africa-Iberia-Adria-Laurentia domains (a) at ~200 Ma, prior to the opening of the Alpine Tethys, and (b) at ~148 Ma [from *Schettino and Turco*, 2011]. Star indicates the location of the study area. IB: Ionian Basin; NA: Northern Adria; and SA: Southern Adria. (c–e) Schematic cross sections illustrating the rift-related evolution of the Adriatic microplate. Note that following complete crustal excision in the Anisian-Ladinian, related to opening of the Meliata Basin (Figure 1c), diffuse crustal stretching is recorded throughout the Adriatic Plate and parts of the future European margin (Figure 1d), prior to rift localization related to the formation of the Alpine Tethys (Figure 1e). Note that vertical scale is 2.5 times horizontal scale.

In this paper the processes responsible for focusing of deformation in the Alpine Tethys system are investigated in the Italian Southern Alps, which sample remnants of the former Alpine Tethys rifted margin. This part of the Alpine realm preserves one of the most extensively studied sections across a complex polyphase rift system, displaying a well-known episode of rift focusing [e.g., *Bertotti et al.,* 1993; *Berra et al.,* 2009] (Figures 1c–1e). The tectonothermal evolution of the crystalline rocks directly underlying the Mesozoic basins has been constrained by means of zircon (U-Th)/He thermochronology, in order to explore its relationships with the available tectonostratigraphic record. Importantly, prerift lower crust can also be accessed in this area, within the widely studied Ivrea Zone [e.g., *Handy et al.,* 1999], as a combined effect of rift-related exhumation and Alpine orogeny. The new data acquired in this study, combined with the large body of preexisting data, provide key insights on the evolving crustal/lithospheric architecture and, by inference, on the mechanisms responsible for the westward migration and subsequent localization of this rift system during the Early to Middle Jurassic.

2. Geological Setting

The Adriatic microplate, which makes up the backbone of the Italian Peninsula, originated through multistage Triassic-Jurassic rifting [e.g., *Gaetani*, 2010] (Figure 1), resulting in nearly complete separation from the neighboring continental plates (see *van Hinsbergen et al.* [2014] for a recent discussion on the debated relationship with the more southerly located African Plate). The Adriatic microplate is commonly subdivided into a northern and southern part (Figure 1), sampled in the Central Alps [*Mohn et al.,* 2012] and throughout the Southern Alps and Apennines, respectively, as a result of Cretaceous-Tertiary inversion of the Alpine Tethys system. The rock types derived from remnants of the former rifted margins and today exposed onto the Adriatic Plate preserve the record of a multistage tectonic evolution, spanning the entire Phanerozoic. In the Southern Alps, which are the main subject of this study (Figure 2), Caledonian high-pressure metamorphism [*Franz and Romer*, 2007], Variscan orogeny, and post-Variscan orogenic collapse [e.g., *Spalla and Marotta*, 2007] were followed by regional-scale wrenching, leading to the development of transtensional basins filled by 1.5–2 km thick Late Permian volcanic-sedimentary sequences (*Cassinis et al.* [2012] for a

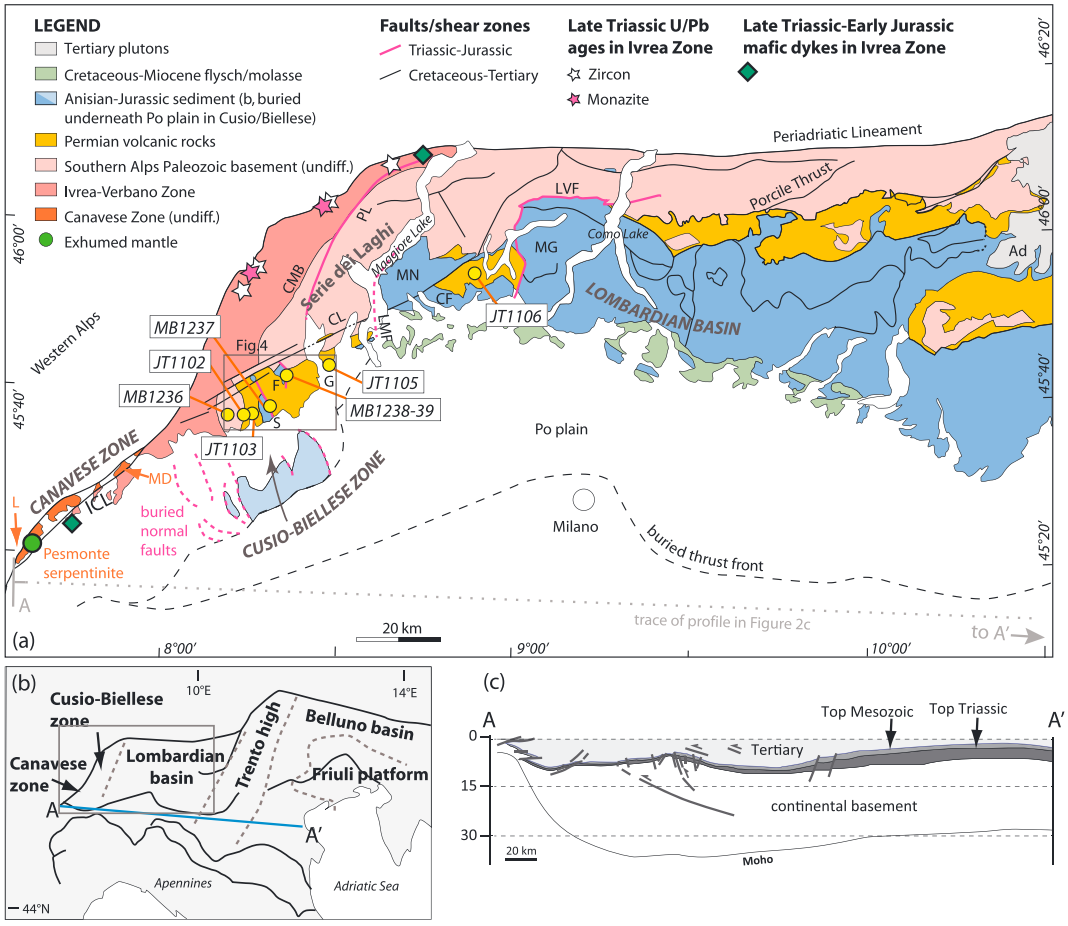

Figure 2. (a) Simplified tectonic map of the western Southern Alps (compiled from *Bigi et al.* [1990], *Handy et al.* [1999], *Fantoni et al.* [2003], and *D'Adda et al.* [2011]). Sampling localities for the ZHe study are indicated by yellow circles. Location of rock specimens from the Ivrea Zone where Late Triassic U-Pb ages have been measured in monazite and zircon is also indicated (see text for references). (b) The main paleogeographic subdivisions of the Southern Alps (modified from *Berra and Carminati* [2010]). (c) The crustal-scale architecture of the Southern Alps along *AA'* profile marked in Figure 2a and 2b [*Turrini et al.,* 2014]. Ad: Adamello batholith; CF: Campo dei Fiori Basin; CL: Cremosina-Marzio Line; CMB: Cossato-Mergozzo-Brissago Line; F: Fenera Basin; G: Gozzano-Invorio ICL: Internal Canavese Line; L: Levone; LMF: Lago Maggiore Fault; MD: Montalto Dora; MG: Monte Generoso Basin; MN: Monte Nudo Basin; PL: Pogallo Line; and S: Sostegno Basin. Brown labels and arrows refer to the different localities of the Canavese Zone mentioned in the text and in Figure 3.

review). These rock types are now the substrate to the Mesozoic rift-related basins (e.g., *Gaetani* [2010] for a review; Figure 2a).

Geophysical studies suggest that the Mesozoic sediments of the Southern Alps are generally underlain by an approximately 20–25 km thick continental crust [e.g., *Turrini et al.,* 2014] (Figure 2c). A marked shallowing of the Moho is observed at the western termination of the Adriatic Plate, in proximity of the Periadriatic Lineament, an Oligocene to lower Miocene mylonitic belt [*Schreiber et al.,* 2010; *Turrini et al.,* 2014]. This feature is generally interpreted as a combined effect of Mesozoic rift-related crustal thinning and rigid body rotation during Alpine continental collision, starting from the Oligocene [e.g., *Schmid et al.,* 1987; *Wolff et al.,* 2012].

Alpine deformation, beginning in the Late Cretaceous [*Meier*, 2003; *Castellarin et al.,* 2006;], led to the development of a south verging fold and thrust belt in the central part of the Southern Alps (Figure 2a). The western part of the Southern Alps, instead, underwent relatively minor Alpine deformation, largely restricted to a few faults and low-temperature shear zones, including the Internal Canavese Line [*Biino and Compagnoni*, 1989], the Cremosina-Marzio fault system [*Boriani and Sacchi*, 1973; *Casati*, 1978], and a NW dipping basal thrust system buried underneath the Po Plain (Figure 2) [*Fantoni et al.,* 2003].

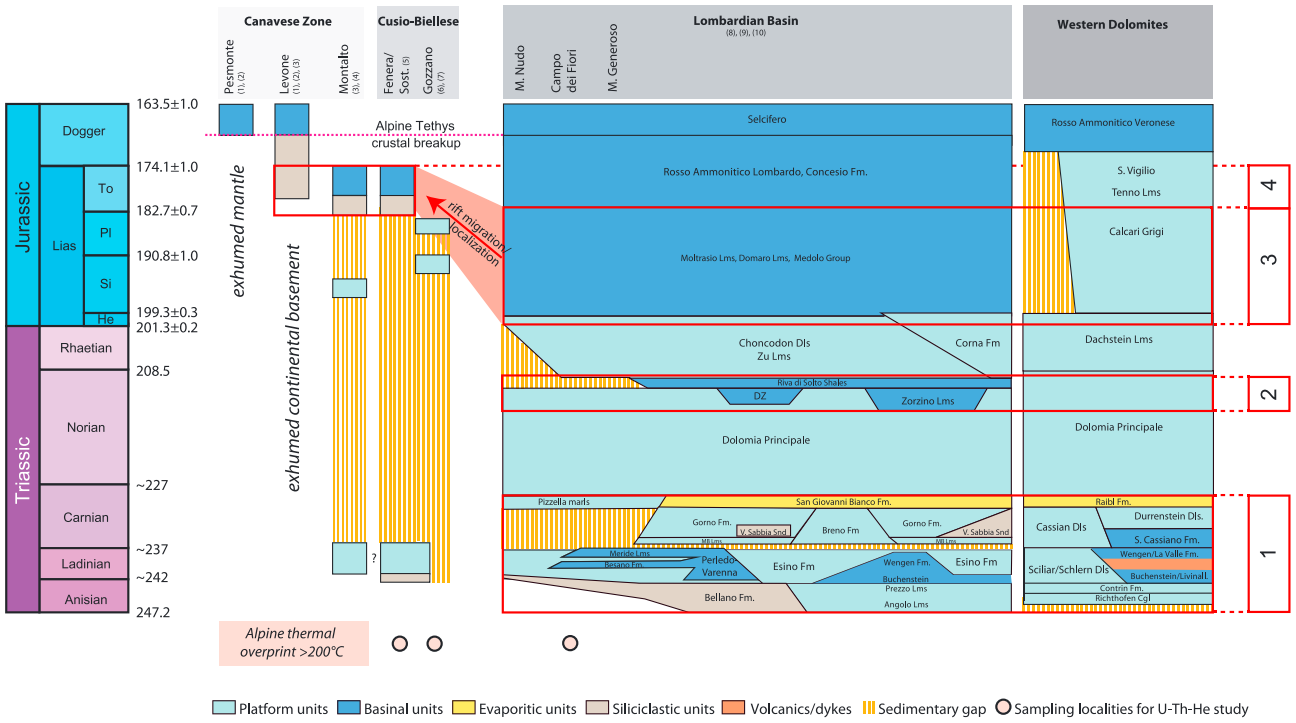

Figure 3. Chronostratigraphic chart of the Triassic to Middle Jurassic sedimentary cover of the Southern Alps, from the Canavese Zone to the Dolomites. The main intervals of extensional faulting discussed in the text are marked by the red rectangles and labeled 1 to 4. Note the westward rift migration episode in the Lower Jurassic. References for the western part of the Lombardian Basin and the Cusio-Biellese-Canavese area are also indicated: (1) *Elter et al.* [1966], (2) *Beltrando et al.* [2015], (3) *Ferrando et al.* [2004], (4) *Sturani* [1964], (5) *Berra et al.* [2009], (6) *Casati* [1978], (7) *Montanari* [1969], (8) *Bertotti et al.* [1993], (9) *Berra et al.* [2009], and (10) *Berra and Carminati* [2010]. Pink circles indicate the basins that have been the subject of this study.

A review of the existing information on the Triassic-Jurassic tectonostratigraphic evolution of the upper crustal levels preserved in the Southern Alps is presented in section 2.1. Section 2.2, instead, is devoted to the Triassic-Jurassic tectonometamorphic evolution of the Ivrea Zone, which, prior to the onset of Tethyan rifting, rested at lower crustal depth, along the future western edge of the Adriatic Plate [e.g., *Handy et al.,* 1999].

2.1. Upper Crustal Rift-Related Tectonostratigraphic Evolution

The Mesozoic tectonostratigraphic evolution of the Southern Alps has long been interpreted as the result of the interaction between two main independent rift systems, whereby Ladinian-Carnian opening of the Meliata and Ionian oceanic branches to the NE and SSE [e.g., *Velledits*, 2006; *Decarlis et al.,* 2013] was followed by opening of the Alpine Tethys domain to the west, in the late Middle Jurassic (Figure 1; see *Gaetani* [2010] for a review). As a result, the Southern Alps preserves the record of the interaction between these two spatially and temporally distinct rift systems.

Several main pulses of extensional tectonics, traditionally bracketed to the Anisian-Carnian, Late Norian, Hettangian-Sinemurian, and Pliensbachian-Toarcian have been identified (Figure 3) [see *Bertotti et al.,* 1993; *Berra and Carminati*, 2010, and references therein]. While Anisian-Carnian rifting has been ascribed to the tectonic evolution of the Meliata system, the subsequent stages, starting from the Late Norian, are generally attributed to the early rifting leading to the opening of the Alpine Tethys [e.g., *Bertotti et al.,* 1993]. Importantly, these different rifting stages are not equally distributed throughout the Southern Alps and evidence for a westward migration of extensional faulting in the Pliensbachian-Toarcian, in the lead up to complete crustal breakup, has been repeatedly provided [*Bertotti et al.,* 1993; *Berra and Carminati*, 2010]. The multistage Triassic-Jurassic tectonic evolution of the Southern Alps led to the development of several basin systems with a distinctive tectonostratigraphic evolution, which, from west to east, are generally grouped within the Canavese Zone, the Cusio-Biellese area, the Lombardian Basin, the Trento High, the Belluno Basin, and the Friuli Platform [*Bertotti et al.,* 1993; *Berra et al.,* 2009] (Figure 2b). A summary of the key elements of the post-Anisian tectonostratigraphic evolution of the western part of the Southern Alps

(Lombardian Basin and Cusio-Biellese-Canavese (CBC) area) is provided here, with a focus on the evidence for westward rift migration and localization in the Lower Jurassic (Figure 3). Readers are referred to *Bertotti et al.* [1993], *Berra et al.* [2009], *Berra and Carminati* [2010], and *Gaetani* [2010, and references therein] for further details. While discussing the stratigraphic data, depositional ages will be presented using the chronostratigraphic nomenclature. Considering that this data set will later be correlated with geochronological data, the absolute timing of deposition/deformation within the sedimentary basins will be provided for the critical stages of their evolution, following *Cohen et al.* [2013, updated in January 2015].

2.1.1. Tectonostratigraphic Evolution of the Lombardian Basin

The earliest evidence for regional-scale rift-related normal faulting within the Southern Alps consists of the horst and graben morphology established in the Anisian, prior to the ubiquitous deposition of the Ladinian peritidal carbonate platform (San Salvatore Dolomite-Esino limestone; Figure 3). This rifting stage was coupled with magmatic activity, as Late Anisian-Early Ladinian tuffs were deposited all over the Southern Alps, from the western [*Carraro and Fiora*, 1974] to the eastern end (see *Gaetani* [2010] for a review). Feeder dykes and intrusive bodies related to this magmatic stage have so far been located only in the Trento High, in the Dolomites, in NE Italy [*Cassinis and Zezza*, 1982].

The subsequent Late Ladinian regional emersion was coupled with renewed extensional tectonics and another magmatic cycle [*Cassinis et al.,* 2008]. Magmatic rocks displaying a calc-alkaline to shoshonitic geochemical affinity [e.g., *Bonadiman et al.,* 1994] were emplaced from the Ladinian-Carnian boundary to the Early Carnian along ENE-WSW strike-slip faults, largely located in the Trento High and Belluno Basin.

This rifting stage was followed by the demise of the carbonate platform in the Late Carnian, coupled with minor basaltic volcanism. As a result, dykes ranging from picrobasalts to phonotephrites, characterized by alkaline to subalkaline composition were emplaced within sedimentary successions throughout the future Lombardian Basin and the Trento High [*Garzanti et al.,* 1995; *Cassinis et al.,* 2008].

Peritidal conditions were reestablished over most of the Southern Alps in the Early Norian, as recorded by the Dolomia Principale platform, prior to renewed E-W regional extension in the Middle-Late Norian [*Picotti and Pini*, 1988; *Jadoul et al.,* 1992]. The resulting morphology, characterized by N-S trending intraplatform basins, was sealed during the subsequent Rhaetian to earliest Hettangian tectonic quiescence stage by shaley limestones (Riva di Solto shales) and platform carbonates (Zu limestone).

Renewed regional extension in the Lombardian Basin, starting in the Hettangian, was accommodated along N-S trending normal faults. As a result, up to 3 km thick sequences of hemipelagic to pelagic spongolitic limestones (Moltrasio limestone) were deposited in half graben basins, including the widely studied Monte Generoso Basin [*Bernoulli*, 1964; *Bertotti*, 1991]. While the main extensional stages ended in the Sinemurian, minor faulting might have taken place up to the Pliensbachian [*Bertotti et al.,* 1993]. No subsequent normal fault activity is documented in the Lombardian Basin (Figure 3).

2.1.2. Tectonostratigraphic Evolution of the Cusio-Biellese-Canavese Area

Several steps of the tectonostratigraphic evolution of the Lombardian Basin illustrated above are missing to the west of the Lake Maggiore (Figure 3), in the Cusio-Biellese and Canavese (CBC) areas (Figures 2 and 4), where the post-Ladinian to pre-Sinemurian sedimentary record is lacking. In the Cusio-Biellese area, Jurassic sediments overlie unconformably the karstified top of the Ladinian San Salvatore platform (Figures 5a and 5b) or the Permian volcanic rocks, indicating that this domain underwent episodic emersion. In the Gozzano-Invorio domain, at the eastern end of the Cusio-Biellese Zone (Figures 2a, 3, and 4), emersion is constrained to pre-Sinemurian times, as Sinemurian shallow marine carbonates were deposited directly onto Permian volcanic rocks [*Montanari*, 1969]. Sinemurian sediment deposition followed erosion of the preexisting Triassic dolostones, now found in a poorly sorted, clast-supported angular breccia resting onto Permian volcanic rocks in Invorio [*Casati*, 1978]. Ladinian to Sinemurian sediments are also lacking at the western end of the CBC area, in the Canavese Zone, where Sinemurian crinoidal limestone overlay the Triassic dolostone, of supposed Ladinian age (Figure 3) [*Sturani*, 1964; *Elter et al.,* 1966].

Sinemurian sedimentation predated the onset of the latest major extensional episode recorded in the Southern Alps, in the Late Pliensbachian-Toarcian, prior to the opening of the Alpine Tethys. Within the CBC area, normal faulting and fault-related topography are testified by the deposition of a shallow water sandstone (San Quirico sandstone), indicative of widespread subaerial exposure of Permian volcanic rocks and metamorphic basement [*Fantoni et al.,* 2003; *Berra et al.,* 2009]. In the Sostegno and Fenera Basins, this

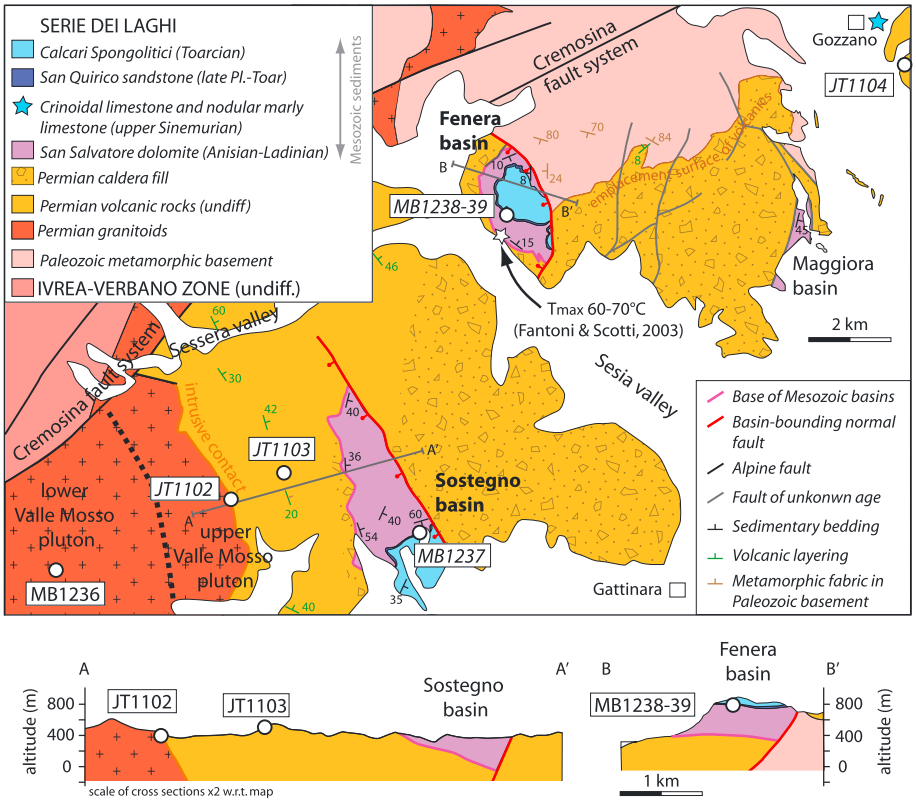

Figure 4. Geological map of the Cusio-Biellese area (compiled from *Carraro et al.* [1967], *Govi* [1977], *Quick et al.* [2009], and own observations). Cross sections *AA*′ and *BB*′ are modified from *Carraro et al.* [1967] and *Fantoni et al.* [2003], respectively. Sampling localities for this ZHe study are indicated.

sandstone rests directly onto the previously emerged Ladinian platform (Figure 5b). The syntectonic depositional environment is confirmed by neptunian dykes related to tectonic brecciation of the Ladinian platform and Sinemurian limestone, partly filled by San Quirico sandstone in the Canavese Zone [*Ferrando et al.,* 2004]. Importantly, while normal faulting was active in the CBC area, where the newly formed half graben basins were filled by Toarcian spongolitic limestone, extension ceased throughout the Lombardian Basin, where pelagic sediments draped the preexisting topography.

Regional exhumation of continental basement to the seafloor [*Ferrando et al.,* 2004] and local evidence of mantle exhumation at the southernmost end of the Canavese Zone [*Elter et al.,* 1966; *Beltrando et al.,* 2015] suggest a southwestward transition to the hyperextended part of the Adriatic margin. This conclusion is supported by the poorly preserved supradetachment basins, hosting continent-derived polymictic breccias of supposed Toarcian to Middle Jurassic age, lying directly onto exhumed continental basement [*Beltrando et al.,* 2015]. The synrift sedimentary succession is then sealed throughout the Southern Alps by post-tectonic sedimentary formations (Radiolarian and Maiolica formations in the Canavese area and the Selcifero group in the Lombardian Basin), of Bathonian to Tithonian age, marking the onset of the post-rift evolution of the Alpine Tethys margin (Figure 3).

Therefore, the extensive body of literature summarized above indicates that the CBC area was originally located at the transition between the proximal Alpine Tethys margin, preserved in the Lombardian Basin, and the future distal margin, best preserved at the southern end of the Canavese Zone. Within this context, the CBC area records a distinctive tectonostratigraphic evolution, related to an episode of westward rift migration in the Lower Jurassic (Figure 3). The shift of upper crustal faulting is bracketed between the Sinemurian and the Late Pliensbachian-Toarcian, when the earliest fault activity has been inferred for the CBC area and no fault activity is documented any longer from the more proximal Lombardian Basin

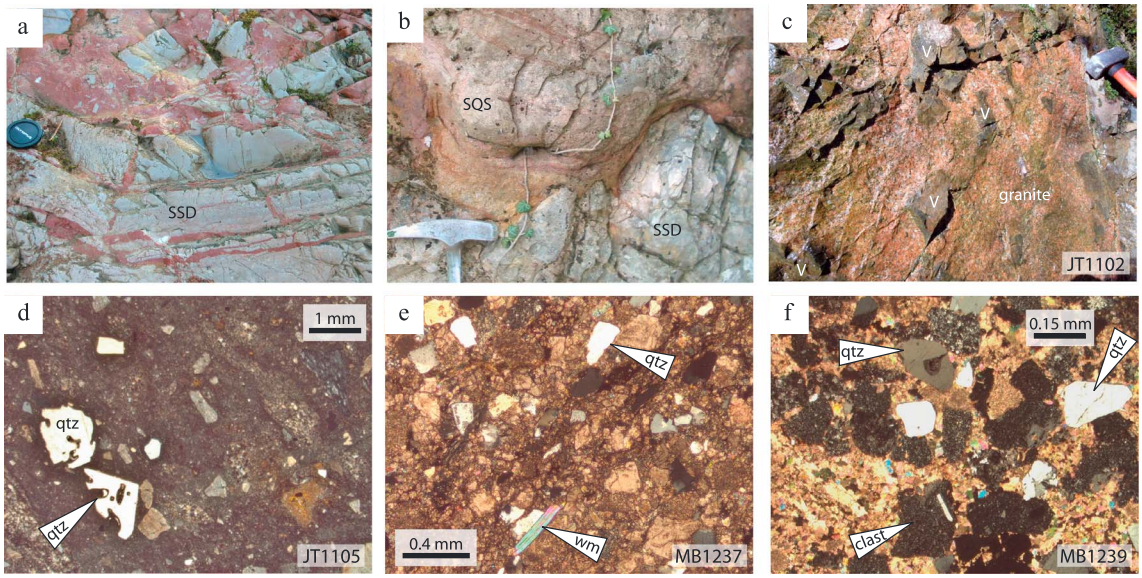

Figure 5. Key lithostratigraphic features of the study area and selected microphotographs of studied samples. (a) Karstification of the Ladinian dolostone (San Salvatore Dolomite: SSD) is indicated by in situ brecciation and filling by the red matrix in the Sostegno Basin. (b) Local evidence of San Salvatore dolostone directly overlain by the Pliensbachian-Toarcian syntectonic San Quirico Sandstone is preserved in the Fenera Basin (photo courtesy of F. Berra). (c) The Permian volcanic rocks underlying the Sostegno Basin are intruded by the Valle Mosso pluton, as indicated by the intrusion breccia in the locality where sample JT1102 was collected. (d) The Permian volcanic sequence consists of lava flows, as shown for sample JT1105, collected near Gozzano, and volcanic breccias. The detrital content of the San Quirico sandstone is heterogeneous, and both minerals originated from the (e) metamorphic basement (sample MB1237) and (f) clasts of Permian volcanic rocks (sample MB1239) may be found alongside carbonate clasts.

[*Bertotti et al.,* 1993]. Extensional deformation in the CBC area, which eventually culminated in mantle exhumation in the Canavese Zone in the Middle Jurassic, was preceded/accompanied by regional emersion.

2.2. Lower Crustal Tectonometamorphic Evolution

Most continental basement units now sampled in the Southern Alps resided at upper crustal depths at the onset of rifting, as indicated by the frequently preserved primary contacts with the Permian lava flows or the subsequent Permian-Triassic sedimentary cover [e.g., *Bigi et al.,* 1990]. The Ivrea Zone, located at the western end of the Southern Alps, provides a notable exception (Figure 2a). This widely studied tectonometamorphic unit preserves a section of Permian lower crust now tilted to the vertical [*Henk et al.,* 1997; *Demarchi et al.,* 1998]. As a result, rocks located at approximately 30 km depth prior to the onset of rifting are now preserved in the proximity of the Periadriatic Lineament, while progressively shallower depths can be accessed farther to the east. The Ivrea Zone is bounded to the east by the so-called Serie dei Laghi, consisting of Paleozoic metamorphic basement, Permian granitoids, and Permian volcanic rocks [e.g., *Boriani et al.,* 1990] onto which the Sostegno and Fenera Basins were established (Figures 2 and 4). The boundary between the Ivrea Zone and the Serie dei Laghi is commonly marked by the Cossato-Mergozzo-Brissago (CMB) line, of Permian age [e.g., *Mulch et al.,* 2002a]. Toward the northern end of the Ivrea Zone, the CMB line is displaced by the younger Pogallo Line [*Handy*, 1987]. Rotation of the western end of the Southern Alps to its current orientation was likely achieved as a combined effect of Jurassic rifting and Alpine tectonics [*Handy et al.,* 1999; *Wolff et al.,* 2012], although the role played by Late Permian transtension is also debated [*Boriani and Giobbi*, 2004].

In the context of the evolution of the western end of the Adriatic Plate, the Ivrea Zone is conveniently located to provide complementary information to the rift-related evolution of the upper crustal domains sampled in the CBC area (Figure 2). Following the widely studied postorogenic Carboniferous to Permian magmatic underplating, coeval with the extensive volcanism seen at the surface [e.g., *Quick et al.,* 2009; *Klötzli et al.,* 2014], the Ivrea Zone records local evidence of intrusions of hydrous melt with tholeiitic to transitional geochemical affinity, now preserved at the northern end of this tectonometamorphic unit, at circa 235–230 Ma [*Zanetti et al.,* 2013]. Following these main pulses of magma emplacement, hot fluid circulation

at lower crustal depth during the uppermost Triassic has been suggested based on several lines of evidence. Most importantly, U-Pb studies on zircon from metapelites and gabbroic rocks from the originally deepest parts of the Ivrea Zone repeatedly yielded a significant uppermost Triassic age cluster, constrained at 210 ± 12 Ma [*Vavra et al.,* 1999], 205 ± 3 Ma [*Zanetti et al.,* 2013], and 220–200 Ma [*Ewing et al.,* 2013] in different localities (Figure 2a). Uppermost Triassic ages are normally determined from featureless zircons and zircon rims, attributed to fluid-mediated recrystallization of preexisting zircon crystals [e.g., *Vavra et al.,* 1999; *Zanetti et al.,* 2013]. A similar interpretation was proposed for the Pb loss event affecting metamorphic monazite at 210 ± 14 Ma [*Vavra and Schaltegger*, 1999].

The timing of regional fluid circulation in the area overlaps with limited evidence for magmatic injections in different parts of the Ivrea Zone: dioritic dykes with a tholeiitic to transitional affinity, for which Sm-Nd three-point isochrones (cpx-plag-WR) yielded crystallization ages of 204 ± 31 Ma and 198 ± 29 Ma, intruded the southern end of the Ivrea Zone [*Mazzucchelli et al.,* 2010]; repeated injections of alkaline melts within the lowermost crust, in the 212–190 Ma interval, are found at the northern end of the Ivrea Zone, near Finero [*Schaltegger et al.,* 2015]. The latter melts, which were formed by low-degree decompression melting of a metasomatically enriched mantle source, point to the existence of a long-lived period of heat advection at deeper crustal levels [*Schaltegger et al.,* 2015]. Interestingly, despite the very limited occurrence of Upper Triassic to Lower Jurassic igneous rocks within the Ivrea Zone and from the Southern Alps at large, Upper Triassic U-Pb ages are common in detrital zircons from an orogeny-related flysch deposit, labeled "Schlieren flysch" currently stacked in the Swiss-French pre-Alps [*Bütler et al.,* 2011]. This Cretaceous to Eocene sedimentary sequence, which was fed from the Southern Alps, yielded a distinctive age peak at circa 205 Ma, suggesting that Upper Triassic magmatism was possibly more extensive than hitherto recognized [*Bütler et al.,* 2011].

The Ivrea Zone is dissected by a number of ductile shear zones, active at granulite to amphibolite facies conditions [e.g., *Rutter et al.,* 1993, 2007], for which limited age data are available. The regional-scale Anzola-Rosarolo shear zone provides a notable exception, as step-heating Ar-Ar geochronology on amphiboles was performed in different localities both by *Brodie et al.* [1989] and *Boriani and Villa* [1997]. Within the Anzola type locality, the shear zone was formed at amphibolite facies conditions at the expense of a preexisting amphibole gabbro [e.g., *Brodie et al.,* 1989], which yielded Ar-Ar ages in the 293–247 Ma range. Younger ages were estimated both from amphibole porphyroclasts within the shear zone, which yielded ages as young as 209 ± 1 Ma (and a 215 ± 5 Ma "plateau" age, if 90% of the released ^{39}Ar is considered) and in a finer-grained mineral separate, consisting both of synkinematic amphibole and porphyroclastic amphibole, which yielded ages in the 208–203 Ma range (52% released ^{39}Ar). *Brodie et al.* [1989] interpreted their data set as recording grain size-dependent partial Ar loss throughout the Triassic affecting amphiboles formed during Permian ductile shearing. However, their interpretation is inconsistent with (1) the marked age difference between the amphibole porphyroclasts within the shear zone and the late-magmatic amphiboles from the country rock, despite the similar grain size, and (2) the nearly identical youngest age steps measured both from the porphyroclastic and the neoblastic amphiboles within the shear zone. Furthermore, step-heating experiments of partly mylonitized amphibolites from a different locality yielded a mixed age spectrum, with the youngest steps at 217 ± 1 Ma [*Boriani and Villa*, 1997], which were interpreted as indicative of the maximum age of synkinematic recrystallization. Therefore, we contend that the existing Ar-Ar geochronological studies on amphibole [*Brodie et al.,* 1989; *Boriani and Villa*, 1997] are best explained collectively as arising from post-Permian amphibole recrystallization along the studied sections of the Anzola-Rosarolo shear zone. Considering the available data, a lower bound to the shear zone activity can be placed at 209 ± 1 Ma, while the upper bound is ill defined, yet younger than 203 Ma. Hence, the Anzola shear zone was (at least partly) active in the 210–200 Ma interval, as also suggested by *Zanetti et al.* [2013] based on different lines of evidence.

Subsequent ductile shearing was accommodated along the Pogallo Line, which crops out at the northern end of the Ivrea Zone and locally marks the boundary with the Serie dei Laghi (Figure 2a) [*Handy*, 1987]. Ar-Ar geochronology on metamorphic white micas formed at the transition between amphibolite and greenschist facies conditions (approximately 500°C) yielded an estimate of 182.0 ± 1.6 Ma for the timing of crystallization [*Mulch et al.,* 2002b]. This estimate is consisted with the crystallization of titanite at 173 ± 4 Ma in the footwall of the shear zone, interpreted to record retrogression arising from cooling [*Mulch et al.,* 2002a]. Cooling of the Ivrea Zone to $T < 500$°C through extensional unroofing is also supported by the oldest U-Pb ages preserved in rutile, which fall in the 185–175 Ma interval [*Zack et al.,* 2011; *Smye and*

Stockli, 2014; *Ewing et al.,* 2015]. Furthermore, a recent U-Pb geochronological study on rutile also suggests that the Ivrea Zone underwent a short-lived heating-cooling cycle at 160 ± 7 Ma [*Ewing et al.,* 2015].

Therefore, the existing geochronological data set from the Ivrea Zone is suggestive of regional-scale hot fluid flow in the 220–200 Ma interval, coupled with minor evidence for magmatism and shear zone activity starting from circa 210 Ma. Subsequent cooling was largely achieved through extensional unroofing starting at circa 185–180 Ma. No evidence of subsequent activity of ductile shear zones has been provided yet.

3. Thermochronometry Sampling Strategy

A new zircon (U-Th)-He data set was acquired at the western end of the Adriatic Plate to constrain the thermal evolution of the upper crust during Mesozoic rifting and hyperextension. This study was designed to bridge the gap between the well-constrained tectonosedimentary evolution of the Lombardian Basin and CBC area and the equally widely studied tectonometamorphic evolution of the originally underlying Ivrea Zone. The main aim of this study consisted in providing a crustal-scale view of the thermotectonic evolution of the Adriatic Plate during the well-documented episode of rift migration and focusing during the Late Triassic to Early Jurassic.

Zircon (U-Th)/He thermochronometry (ZHe), with a thermal sensitivity window between 200 and 130°C, was selected to unravel the Mesozoic synextensional thermal evolution of this domain. This choice was dictated by the interplay between the shallow paleodepth of the rocks available for this study, excluding the possibility of rift-related resetting of medium- to high-temperature thermochronometers, and the documented Alpine thermal evolution. Published studies outline a westward increase in Alpine thermal overprint between the Maggiore Lake and the Periadriatic Lineament (Figure 2a), as low organic matter maturity indicates maximum temperatures of 60–70°C in the Anisian sediments of the Fenera Basin [*Fantoni and Scotti*, 2003], while anchizonal metamorphic conditions (approximately 250–300°C) were reached in the Canavese Zone [e.g., *Biino and Compagnoni*, 1989; *Vance*, 1999].

Samples of Permian volcanic rocks, Permian granitoids, and synrift sandstones were collected systematically along an ENE-WSW oriented transect, perpendicular to the early Mesozoic rift-related structural grain, from the immediate footwall of the Monte Generoso Basin, at the western end of the Lombardian Basin, to the westernmost part of the Serie dei Laghi, in proximity of the Cremosina-Marzio fault system (Figures 2a and 4 and Table 1). The documented Alpine partial resetting of zircon fission track ages in more westerly located areas [e.g., *Vance*, 1999; *Siegesmund et al.,* 2008; *Wolff et al.,* 2012] prevented sample collection from more distal domains of the Adriatic margin. Basement samples were collected from areas directly adjacent to Mesozoic sedimentary basins, in order to allow reliable estimates of their overburden throughout the Triassic-Jurassic, based on preexisting studies of these weakly deformed domains (Figure 4 and Table 1). Sampling was mostly focused in direct proximity of the Sostegno and Fenera Basins, where a 2.3–2.4 km thick sequence of Permian volcanic rocks, emplaced in the 290–280 Ma interval onto Paleozoic metamorphic basement, was intruded at 280–270 Ma by the Valle Mosso pluton [*Govi*, 1977; *Quick et al.,* 2009]. Intrusion breccias are preserved at the eastern margin of this pluton (Figure 5c), where myarolitic cavities, indicative of emplacement at epiplutonic conditions, are common [*Zezza et al.,* 1984].

Mesozoic sediments deposited onto the volcanic rocks are found in several localities throughout this area (Figure 4), being best exposed in the Sostegno and Fenera Basins, where their thickness can be estimated. As a result, the burial depth of basement samples throughout the Triassic-Jurassic can be estimated considering their distance from the base of the Mesozoic basins as well as the attitude of the interface between volcanic rocks and Mesozoic sediments. The overburden at the Triassic-Jurassic boundary for each sample is reported in Table 1. In the Fenera Basin, volcanic rocks are directly overlain by a few meters of shallow water sandstone then followed upward by a few tens of meters of Anisian marly limestone, approximately 300 m of Ladinian dolostone, capped upward by the karst. The latter is directly overlain by approximately 30–40 m of San Quirico sandstone, locally containing wood fragments, which then gives way to deep water marls and turbiditic sandstones (*Calcari Spongolitici*). The fossil content of the postkarst sediments suggests a Late Pliensbachian to Toarcian age of deposition [*Berra et al.,* 2009]. Both the Sostegno and Fenera Basins are bounded to the NE by SW dipping normal faults, interpreted as original synrift faults, likely partially reactivated during Cretaceous to Tertiary Alpine tectonics.

Table 1. Sample List, Including Rock Type, Sample Location, and Estimated Overburden at the Triassic-Jurassic Boundary[a]

Sample #	Rock Type	Location	GPS (Longitude; Latitude)	Crystallization/Depositional Age	Thickness of Overlying Volcanic Rocks	Thickness of Triassic Sediments	Maximum Overburden at Triassic-Jurassic Boundary
MB1236	Granite	Maglione Crosa	0433612; 5050310	278 ± 5 Ma [*Quick et al.*, 2009]	Maximum approximately 8 km	300 m [*Berra et al.*, 2009]	<8300 m
JT1102	Granite	San Bonomio quarry	0439666; 5054005	278 ± 5 Ma [*Quick et al.*, 2009]	2300–2400 m	300 m [*Berra et al.*, 2009]	2600–2700 m
JT1103	Ignimbrite	Olzera	0441029; 5054644	290–280 Ma [*Quick et al.*, 2009]	1100–1200 m	300 m [*Berra et al.*, 2009]	1400–1500 m
JT1105	Ignimbrite	Briga Novarese quarry	0457496; 5065166	Undated (part of the Permian volcanics)	Unknown (maximum 2300–2400 m)	Unknown (maximum 300 m)	Unknown (max 2600–2700 m)
JT1106	Lava flow	Valganna	0486843; 5084188	298–281 Ma [*Schaltegger and Brack*, 2007]	Approximately 2000 m [*Schaltegger and Brack*, 2007]	1000–1500 m [*Desio*, 1973]	3500 m
MB1237	S. Quirico sandstone	Casa del Bosco (Sostegno Basin)	0444508; 5053068	Late Pliensbachian-early Toarcian [*Berra et al.*, 2009]			
MB1238	S. Quirico sandstone	San Quirico (Fenera Basin)	0446710; 5061389	Late Pliensbachian-early Toarcian [*Berra et al.*, 2009]			
MB1239	S. Quirico sandstone	San Quirico (Fenera Basin)	0446720; 5061263	Late Pliensbachian-early Toarcian [*Berra et al.*, 2009]			

[a]Overburden was estimated from existing studies providing the thickness of the Permian volcanic sequence and of the Triassic carbonates, considering the present-day attitude of the sedimentary layers (from *Carraro et al.* [1967] and *Govi* [1977] and own observations shown in Figure 4), which are treated as subhorizontal marker horizons at the time of deposition. The overburden inferred with this methodology should slightly underestimate the actual value, due to the likely removal of part of the Triassic sedimentary cover during post-Ladinian emersion. However, the limited extent of karstification and brecciation of the Ladinian carbonatic platform [*Berra et al.*, 2009] suggests that only limited erosion took place. Sample location is given in UTM WGS84 32N coordinates.

Three samples (MB1236, JT1102, and JT1103) were collected at increasing paleodepths within the crystalline substrate of the Sostegno Basin, where the deepest crustal levels are accessible, thanks to the Alpine rotation of the crustal section, indicated by the ~40° dip of the sedimentary strata and volcanic layers (Figure 4). A biotite- and white mica-bearing monzogranite (MB1236) and a granite from the intrusive contact with the Permian lava flows (JT1102) were sampled from the Valle Mosso pluton. Furthermore, sample JT1103 was collected from the Permian volcanic-sedimentary sequence within the Sesia caldera [*Quick et al.*, 2009], halfway between sample JT1102 and the base of the Sostegno Basin. This Permian ignimbrite hosts xenoliths of porphyric volcanic rocks and, more rarely, metamorphic basement with a maximum size of several centimeters, into a matrix consisting of devitrified volcanic glass. The overburden of samples JT1102 and JT1103 at the Triassic-Jurassic boundary was estimated at approximately 2800 m and 1400–1500 m, respectively. The burial depth of sample MB1236, which lies deep into the Valle Mosso pluton, toward the contact with the underlying metamorphic basement, cannot be estimated precisely. A maximum depth of approximately 8 km is suggested based on its distance from the intrusive contact with the volcanic rocks and on the approximately 35° tilt of the eastern part of the pluton.

A sample of Permian rhyolitic ignimbrite (Figure 5d) was then collected from the Gozzano-Invorio area (JT1105), approximately 10 km to the NE of the Sostegno Basin. Sample paleodepth at the Triassic-Jurassic boundary is unknown, due to the lack of a Triassic sedimentary cover in the Gozzano-Invorio high (see previous section). However, considering the maximum thickness of the Permian volcanic sequence in the western part of the Southern Alps and the thickness of the Triassic sediments in the neighboring Fenera Basin, a maximum overburden of approximately 2800 m can be reasonably suggested for this sample. One more sample of Permian volcanoclastic lava flow, entraining clasts of the directly underlying metamorphic basement (JT1106), was collected from the base of the volcanic sequence, underneath

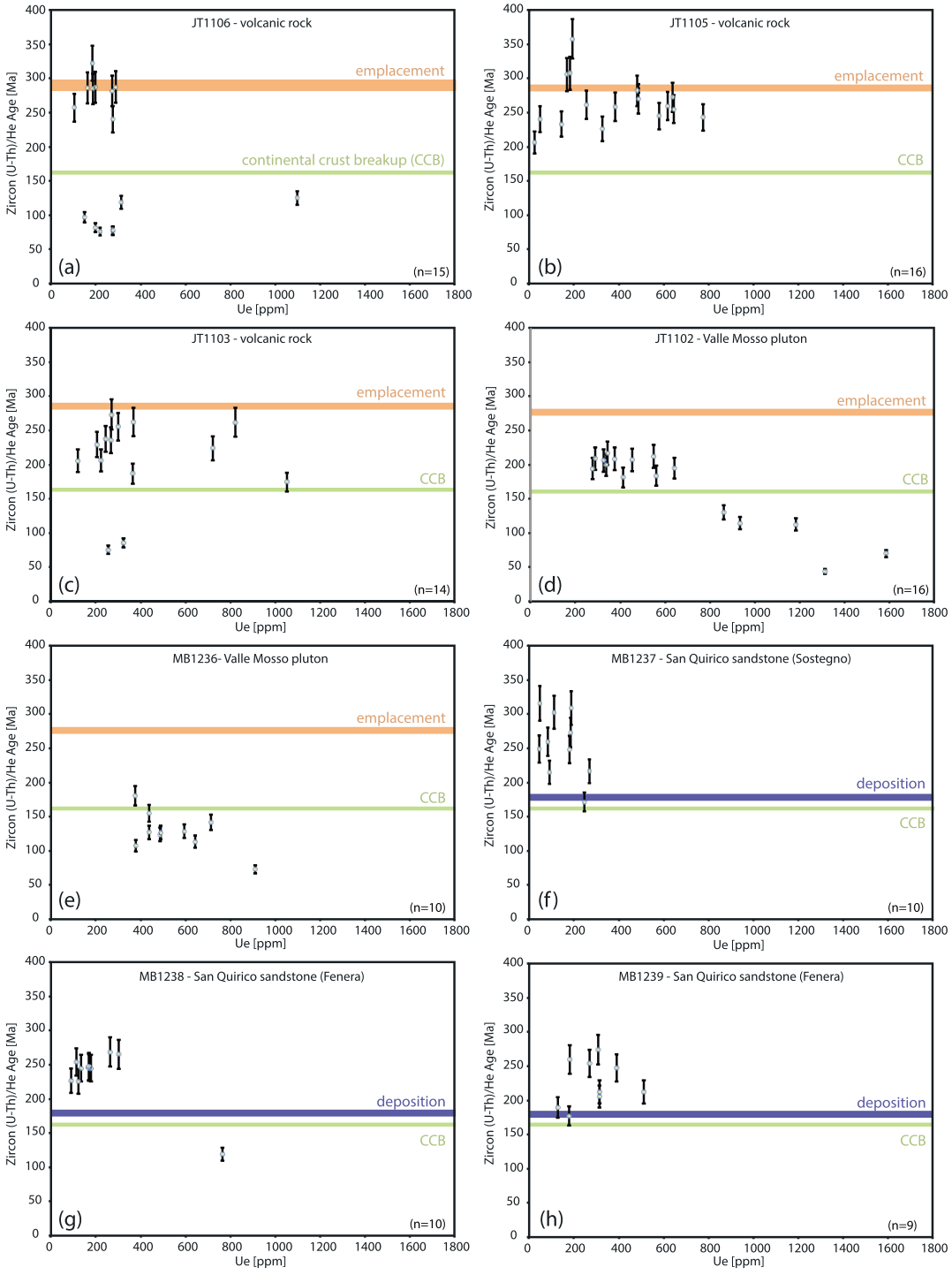

Figure 6. Diagram showing all individual bedrock and detrital zircon (U-Th)/He data plotted against effective uranium (Ue) concentrations. All errors are 2σ. Brown and blue bars denote emplacement (crystallization) ages for bedrock samples and depositional age for detrital samples, respectively. The timing of continental crust breakup (CCB) is provided for reference.

the Campo dei Fiori Basin, at the western edge of the Lombardian Basin. An overburden of approximately 3500 m is estimated for this sample.

Furthermore, three samples of San Quirico sandstone, the Late Pliensbachian-Toarcian deposit directly resting onto karstified Ladinian dolostone of the Sostegno (MB1237) and Fenera Basins (MB1238 and MB1239), were

collected in order to constrain the main phases of tectonic activity by means of lag time estimates. MB1237 consists of angular to weakly rounded clasts of carbonates (>70%), quartz (approximately 20%), minor white mica, chloritized biotite, and feldspar (Figure 5e). The presence of white mica, biotite, and quartz crystals with a subgrain microstructure indicates sourcing from the metamorphic basement, alongside the pre-Jurassic sedimentary cover. MB1238 and MB1239 were collected from the type locality of the San Quirico sandstone, on Monte Fenera. MB1239 consists largely of carbonates (approximately 50%) and hosts millimeter-sized angular clasts of volcanic rocks, consisting of a porphyric quartz into a fine-grained matrix, and subvolcanic rocks, with vermicular quartz + k-feldspar, alongside several quartz crystal displaying either the trigonal pyramid termination or crystal margins with marked embayments (Figure 5f). Both features are typical of volcanic quartz. The detrital content, as well as the preservation of original crystal edges, indicates that the studied sandstone was sourced locally, possibly mostly from the Permian volcanic rocks found directly aside the Fenera Basin.

4. Bedrock and Detrital Zircon (U-Th)/He Results

The ZHe thermochronometry results are presented from east to west, i.e., from the proximal to the distal Southern Alpine rifted margin, for bedrock and detrital samples (Figure 6 and Table 2). The reader is referred to the supporting information for details on the analytical techniques.

Sample JT1106 is the most proximal bedrock sample and shows two distinct ZHe age populations that do not correlate with Ue or grain size. The primary ZHe population clusters at 288–280 Ma. A second ZHe age population clusters at 82–74 Ma (Figure 6a and Table 2).

Sample JT1105 yields a relatively broad ZHe age scatter, with a handful ($n = 3$) of Carboniferous ages and the rest of the data set ($n = 13$) scattered between 260 and 205 Ma, with a prominent age cluster at 250–255 Ma (Figure 6b). No clear Ue or grain size correlation with ZHe age is observed.

The high age scatter already apparent in JT1105 is even more pronounced in sample JT 1103, collected at a paleodepth of approximately 1.1–1.2 km below the base of the Sostegno Basin (Figure 6c). This sample displays a ZHe age distribution characterized by both Permian and Triassic ages, with an older ZHe population at 275–260 Ma, similar to proximal margin samples (JT1005/JT1006), and a younger population spread out in the 230–200 Ma interval, suggestive of severe partial resetting. Furthermore, two younger ages in the 70–90 Ma interval were also detected.

Sample JT1102, located about 2 km west of JT1103, at an estimated paleodepth of 2.6–2.7 km, shows no Permian ZHe ages (Figure 6d). Importantly, this sample only shows a dominant Triassic age cluster at 215–195 Ma. Therefore, sample JT1102 appears to be completely reset, and no correlation between the Triassic ZHe ages and Ue or grain size is observed. As observed in other samples, JT1102 shows several Cretaceous ZHe ages ($n = 5$), in the 117–80 Ma range, which are clearly related to zircons with very high Ue (850–1600 ppm), suggesting lower thermal sensitivity.

Sample MB1236, located approximately 5 km to the west of JT1102, yielded ZHe ages ranging from 181 ± 15 Ma to 73 ± 6 Ma, with a clear inverse relationship between Ue and ZHe age (Figure 6e and Table 2).

Three sandstone samples deposited in the Upper Pliensbachian-Toarcian in the Fenera and Sostegno Basins yielded detrital ZHe ages that are equal to or older than the depositional age (Figures 6f–6h). Two samples from the Fenera Basin (MB1238 and MB1239) exhibit detrital ZHe ages ranging from circa 270 Ma to 180–170 Ma, with the youngest detrital ZHe ages (177 ± 14 Ma) being indistinguishable from the Late Pliensbachian-Toarcian depositional age (Figures 6g and 6h) [*Berra et al.,* 2009]. Significantly, sample MB1239 yielded a distinctive age cluster at circa 205–212 Ma ($n = 3$). Similarly, a sandstone sample from the Sostegno Basin (MB1237) exhibits a broad range of detrital ZHe ages, from circa 310 Ma to circa 170 Ma, with the youngest age (171 ± 14 Ma) indistinguishable from the depositional age (Figure 6f).

5. Discussion

5.1. ZHe Data Interpretation

5.1.1. Probability Density Plots

Probability density plots (PDPs) were generated with DensityPlotter [*Vermeesch*, 2012] for the entire data set and for selected subsets (Figure 7) to assess the significance of the age populations detected with the qualitative data analysis presented above. When the whole data set is taken together ($n = 100$), four main

Table 2. Single-Grain Zircon (U-Th)/He Age From All Bedrock and Detrital Samples for This Study[a]

	Zircon (U-Th)/He Data									
Sample	Age (Ma)	2σ (Ma)	U (ppm)	Th (ppm)	Ue (ppm)	Th/U	He (nmol/g)	Mass (μg)	Ft	ESR
					JT1102					
JT1102-1	208.4	16.7	338.7	163.1	376.3	0.48	356.7	13.13	0.83	70.2
JT1102-2	208.9	16.7	257.3	141.0	289.8	0.55	257.0	6.37	0.77	52.3
JT1102-3	199.4	16.0	316.7	86.9	336.8	0.27	286.2	5.70	0.78	52.6
JT1102-4	129.9	10.4	738.8	533.2	861.6	0.72	424.2	2.42	0.70	37.9
JT1102-5	112.4	9.0	1109.3	324.1	1184.0	0.29	528.8	3.36	0.73	42.5
JT1102-6	183.6	14.7	494.3	289.9	561.1	0.59	375.7	1.81	0.67	34.1
JT1102-7	206.9	16.5	397.9	239.4	453.1	0.60	340.0	1.61	0.66	33.7
JT1102-8	194.3	15.5	240.6	158.4	277.1	0.66	224.2	4.53	0.76	49.3
JT1102-12	114.4	9.2	848.0	376.0	934.6	0.44	402.8	2.28	0.69	37.1
JT1102-13	194.8	15.6	567.9	325.9	643.0	0.57	442.5	1.50	0.65	31.9
JT1102-14	43.6	3.5	1206.8	461.5	1313.1	0.38	213.7	2.06	0.69	36.5
JT1102-15	181.1	14.5	370.9	183.5	413.2	0.49	307.8	4.27	0.75	47.2
JT1102-17	205.9	22.9	299.4	112.5	325.4	0.38	359.7	2.47	0.70	38.4
JT1102-18	212.2	17.0	469.2	347.5	549.2	0.74	472.3	4.01	0.74	45.1
JT1102-19	216.8	20.5	304.8	163.3	342.4	0.54	361.9	4.27	0.75	46.5
JT1102-20	70.0	5.6	1467.4	516.8	1586.4	0.35	440.2	3.81	0.73	42.8
					JT1103					
JT1103-1	205.4	16.4	94.8	98.2	117.4	1.04	101.3	5.81	0.77	51.0
JT1103-2	174.4	14.0	970.2	345.6	1049.8	0.36	754.1	4.83	0.75	47.2
JT1103-3	235.6	18.9	230.3	152.8	265.5	0.66	257.5	5.09	0.75	47.0
JT1103-4	261.8	20.9	756.6	280.3	821.1	0.37	871.1	4.09	0.74	44.0
JT1103-5	273.2	21.9	233.3	147.9	267.4	0.63	301.7	4.98	0.75	47.1
JT1103-6	262.5	21.0	325.5	176.7	366.2	0.54	391.7	4.20	0.74	45.0
JT1103-7	206.2	16.5	190.0	138.0	221.8	0.73	181.7	4.32	0.73	42.5
JT1103-8	229.4	18.3	177.3	105.6	201.6	0.60	191.5	4.67	0.75	47.9
JT1103-9	186.9	15.0	331.7	133.5	362.4	0.40	294.0	9.14	0.79	57.0
JT1103-10	223.8	17.9	660.0	257.5	719.3	0.39	686.5	7.60	0.78	52.7
JT1103-11	75.5	6.0	216.0	158.2	252.5	0.73	79.5	6.30	0.77	51.0
JT1103-12	255.5	20.4	273.8	98.1	296.4	0.36	333.0	8.05	0.80	58.8
JT1103-14	85.8	6.9	279.5	182.1	321.4	0.65	112.6	4.55	0.75	47.4
JT1103-16	237.8	19.0	215.7	113.5	241.8	0.53	234.0	3.89	0.74	45.1
					JT1105					
JT1105-1	305.7	24.5	145.6	59.5	159.3	0.41	204.9	5.01	0.76	49.2
JT1105-2	206.1	16.5	19.4	8.8	21.4	0.46	19.1	7.96	0.79	56.4
JT1105-3	261.5	20.9	221.7	88.9	242.2	0.40	265.8	5.65	0.76	49.3
JT1105-4	307.4	24.6	159.7	60.4	173.6	0.38	241.7	13.24	0.82	65.8
JT1105-5	281.8	22.5	428.5	139.3	460.6	0.32	561.4	7.43	0.79	54.5
JT1105-6	270.0	21.6	431.4	151.9	466.3	0.35	563.4	10.97	0.81	63.1
JT1105-9	272.3	21.8	537.5	335.0	614.7	0.62	693.2	4.59	0.75	47.5
JT1105-14	258.2	20.7	334.0	143.5	367.0	0.43	415.8	8.38	0.80	58.4
JT1105-16	259.7	20.8	549.5	180.9	591.2	0.33	658.1	6.72	0.78	53.0
JT1105-17	357.7	28.6	165.9	72.5	182.6	0.44	271.5	4.85	0.75	46.7
JT1105-19	242.9	19.4	689.4	243.6	745.5	0.35	740.7	4.57	0.75	45.4
JT1105-20	226.0	18.1	287.1	110.4	312.5	0.38	281.6	3.98	0.73	42.2
JT1105-22	245.0	19.6	505.1	224.4	556.8	0.44	572.6	5.55	0.76	49.6
JT1105-23	233.0	18.6	114.8	93.1	136.2	0.81	130.6	4.31	0.75	47.2
JT1105-24	240.6	19.2	35.7	32.4	43.1	0.91	41.2	3.48	0.72	42.4
JT1105-25	255.0	20.4	564.1	235.3	618.3	0.42	614.9	2.87	0.71	39.5
					JT1106					
JT1106-1	322.4	25.8	167.7	111.9	193.4	0.67	259.6	5.46	0.75	47.8
JT1106-2	286.7	22.9	183.7	94.7	205.6	0.52	247.6	6.04	0.76	49.5
JT1106-3	125.0	10.0	995.9	404.0	1088.9	0.41	601.0	12.55	0.81	62.6
JT1106-4	287.3	23.0	269.9	108.2	294.8	0.40	364.2	7.38	0.78	53.4
JT1106-5	240.1	19.2	258.2	111.7	283.9	0.43	275.9	3.92	0.74	44.2
JT1106-6	284.6	22.8	180.3	69.3	196.2	0.38	257.0	16.89	0.83	72.0
JT1106-7	286.3	22.9	150.9	89.4	171.5	0.59	198.4	4.67	0.73	43.8
JT1106-8	76.1	6.1	201.4	108.9	226.5	0.54	72.9	6.89	0.78	53.5
JT1106-9	76.9	6.2	226.8	247.2	283.8	1.09	89.1	5.40	0.75	47.7

Table 2. (continued)

Zircon (U-Th)/He Data										
Sample	Age (Ma)	2σ (Ma)	U (ppm)	Th (ppm)	Ue (ppm)	Th/U	He (nmol/g)	Mass (μg)	Ft	ESR
JT1106-10	77.8	6.2	264.7	80.4	283.2	0.30	91.3	5.23	0.76	49.1
JT1106-11	81.8	6.5	189.7	76.5	207.4	0.40	70.9	6.98	0.77	51.0
JT1106-12	257.1	20.6	103.1	48.1	114.2	0.47	127.3	7.28	0.79	55.9
JT1106-13	118.7	9.5	291.2	124.6	319.9	0.43	148.7	3.40	0.72	41.0
JT1106-15	281.7	22.5	258.2	96.6	280.4	0.37	348.7	9.83	0.80	59.3
JT1106-16	97.1	7.8	144.5	69.4	160.5	0.48	66.2	7.01	0.78	54.1
MB1236										
MB1236-1	113.2	9.1	576.3	181.5	618.1	0.31	285.7	4.48	0.75	46.4
MB1236-2	141.7	11.3	645.8	181.4	687.6	0.28	421.5	9.23	0.79	56.7
MB1236-3	180.6	14.5	331.8	122.9	360.1	0.37	264.3	3.89	0.74	45.1
MB1236-4	154.9	12.4	392.7	112.8	418.6	0.29	267.7	4.63	0.76	47.6
MB1236-5	123.8	9.9	436.6	132.5	467.1	0.30	241.6	5.24	0.77	50.0
MB1236-6	107.7	8.6	344.7	76.0	362.2	0.22	160.8	4.51	0.76	47.7
MB1236-7	72.8	5.8	847.4	139.6	879.5	0.16	248.2	2.68	0.72	39.7
MB1236-8	126.7	10.1	440.5	123.0	468.8	0.28	250.7	7.22	0.78	51.7
MB1236-9	128.7	10.3	555.6	71.1	572.0	0.13	314.4	6.16	0.78	53.6
MB1236-10	127.1	10.2	403.9	68.5	419.6	0.17	239.1	12.85	0.82	66.4
MB1237										
MB1237-1	247.9	19.8	184.9	26.0	190.9	0.14	214.0	13.36	0.82	66.1
MB1237-2	215.1	17.2	96.2	8.9	98.3	0.09	88.0	5.29	0.76	47.6
MB1237-3	315.5	25.2	49.5	18.9	53.9	0.38	76.2	11.59	0.81	62.6
MB1237-4	248.5	19.9	48.6	15.9	52.3	0.33	58.2	10.23	0.81	63.9
MB1237-5	216.3	17.3	273.2	36.9	281.7	0.14	263.6	7.56	0.79	54.9
MB1237-6	308.9	24.7	181.6	72.2	198.2	0.40	260.9	7.28	0.77	51.3
MB1237-7	273.1	21.9	184.4	46.4	195.1	0.25	245.3	16.53	0.84	72.0
MB1237-8	171.3	13.7	240.7	80.3	259.2	0.33	190.4	7.00	0.79	54.6
MB1237-9	302.4	24.2	114.5	28.8	121.1	0.25	158.7	7.02	0.79	54.3
MB1237-10	259.6	20.8	81.6	40.3	90.9	0.49	101.1	6.83	0.78	53.4
MB1238										
MB1238-1	244.4	19.5	140.2	73.6	157.1	0.53	156.3	4.82	0.74	45.1
MB1238-2	226.5	18.1	64.5	55.1	77.2	0.85	72.0	4.70	0.75	47.4
MB1238-3	264.7	21.2	239.0	123.0	267.3	0.51	295.2	5.06	0.76	48.5
MB1238-4	268.2	21.5	221.0	54.6	233.6	0.25	276.7	8.89	0.80	59.3
MB1238-5	118.4	9.5	602.5	329.4	678.5	0.55	321.2	3.41	0.73	43.7
MB1238-6	244.3	19.5	111.2	30.3	118.2	0.27	118.7	3.99	0.75	45.9
MB1238-7	225.0	18.0	92.2	67.8	107.8	0.73	105.9	7.81	0.79	58.3
MB1238-8	245.6	19.6	132.7	71.9	149.3	0.54	144.3	2.87	0.72	40.8
MB1238-9	253.7	20.3	85.8	53.1	98.0	0.62	105.0	6.06	0.77	50.8
MB1238-10	247.0	19.8	136.0	53.1	148.3	0.39	153.0	4.97	0.76	48.7
MB1239										
MB1239-1	205.2	16.4	283.5	119.2	311.0	0.42	254.2	3.27	0.73	42.4
MB1239-2	253.7	20.3	230.0	162.1	267.3	0.70	269.1	3.22	0.72	42.0
MB1239-3	259.2	20.7	165.3	60.5	179.2	0.37	212.8	14.14	0.83	71.0
MB1239-4	274.0	21.9	269.2	156.1	305.2	0.58	350.8	5.58	0.76	49.4
MB1239-5	189.4	15.2	104.7	87.9	125.0	0.84	96.0	3.97	0.74	45.4
MB1239-7	211.9	17.0	456.0	235.7	510.3	0.52	448.8	4.68	0.76	48.3
MB1239-8	212.2	17.0	276.3	155.2	312.0	0.56	269.1	4.01	0.74	45.2
MB1239-9	247.0	19.8	335.6	225.5	387.6	0.67	392.1	4.83	0.75	46.2
MB1239-10	177.1	14.2	159.4	78.3	177.5	0.49	129.0	4.90	0.75	46.9

[a]Ue is the effective U concentration where Ue = [U] + 0.235[Th]; Ft is the alpha ejection correction calculated using an approach modified after *Farley et al.* [1996]; *n* denotes the number of single-grain zircon aliquot analyses; and ESR is the equivalent spherical radius of the zircon grains. Estimated analytical uncertainty of ~8% (2σ) is based on a decade of replicate analysis of Fish Canyon Tuff ZHe age standard (28.2 ± 2.3 Ma; $n > 2200$). All zircon analyses were completed at the UTChron Geo- and Thermochronometry Laboratory at the University of Texas at Austin.

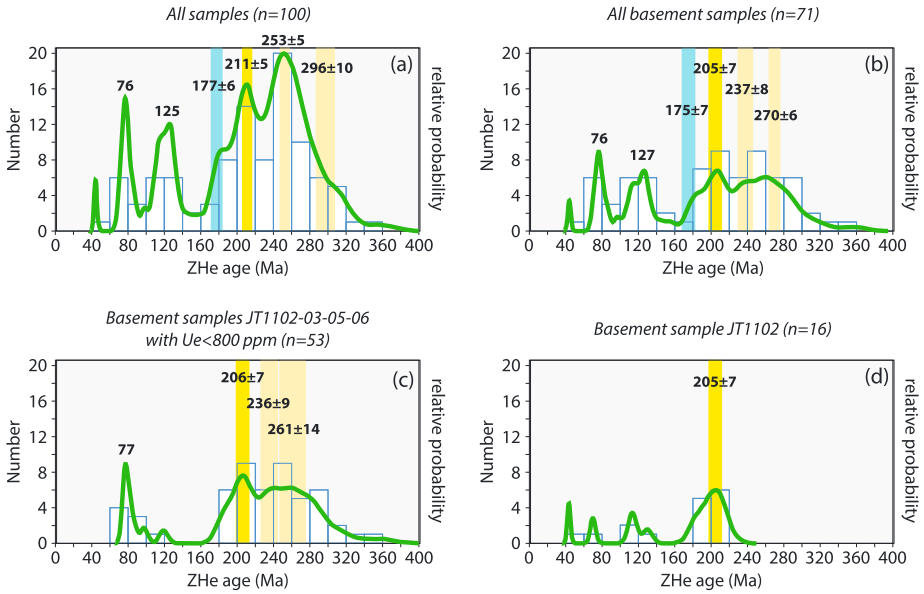

Figure 7. Probability density functions for ZHe age from the Southern Alps. Colored vertical rectangles show the ages (annotated with 2σ errors) obtained by the unmix ages function of Isoplot [*Ludwig*, 2003]. Histogram bin size is 20 Myr. Note that the calculation of the probability density function relies only on individual dates and their errors and is completely independent of bin size. It is therefore more robust than the histogram, which also does not take into account the precision of individual analyses. Histograms are included only to illustrate the number of analyses.

age peaks at ~251 Ma, ~209 Ma, ~125 Ma, and ~76 Ma are detected (Figure 7a). The broad tailing of the ~251 Ma and ~209 Ma peaks toward older and younger ages, respectively, suggests that additional age populations that are not resolved at the precision of the analyses are present within the PDP. Therefore, the "unmix ages" function [*Sambridge and Compston*, 1994], as implemented in IsoPlot 3 [*Ludwig*, 2003], was used on the data subset with ZHe ages >150 Ma, thus removing the already resolved age peaks from the computation. The unmix ages method was designed to extract age populations that are not clearly resolved by partly overlapping individual analyses [*Sambridge and Compston*, 1994]. This method, applied to our data set, results in the detection of two additional age populations at 177 ± 6 Ma and 296 ± 10 Ma (Figure 7a). The 177 ± 6 Ma age population corresponds to an inflection on the PDP, consistent with a partially resolved age peak, while the 296 ± 10 Ma population falls within the broad tailing of ages that implies the presence of more than one single Gaussian population. The ages of the dominant peaks recalculated with the same method, at 211 ± 5 Ma and 253 ± 5 Ma, are indistinguishable from those estimated from the PDP alone.

Considering that this study was mainly aimed at constraining the thermal history of the basement rocks directly underlying the Mesozoic basins, a PDP was also generated for the data subset consisting of all basement samples ($n = 71$; Figure 7b), yielding similar results to the PDP of the complete data set. Furthermore, if the data set in the 150–300 Ma range is analyzed with the unmix ages method, four main age populations are identified at 175 ± 7 Ma, 205 ± 7 Ma, 237 ± 8 Ma, and 270 ± 6 Ma. While the younger age populations (175 ± 7 Ma and 205 ± 7 Ma) are indistinguishable from those determined for the whole data set, the older ones differ considerably, being generally younger. This is interpreted as the combined effect of removal of the detrital zircons yielding ages >300 Ma, which are common in the syntectonic sandstone, as well as partial resetting in the Late Triassic (see discussion in section 5.1.2).

Considering that a negative correlation between Ue and ZHe ages was clearly detected in MB1236 and for all crystals with Ue >800 ppm from sample JT1102, a further sample subset ($n = 53$) was plotted, considering only basement zircons with Ue < 800 ppm and excluding sample MB1236 (Figure 7c). This approach was aimed at filtering out potentially spurious ages, arising from incomplete resetting of older age reservoirs. This approach is supported by the wealth of studies indicating that radiation damage likely results in a substantial decrease in He retentivity, for zircons containing Ue > 800 ppm [e.g., *Guenthner et al.,* 2014]. The resulting disappearance of the 120–130 Ma age peak lends support to this view, further suggesting that this

age mode has no geological meaning. The remaining age peaks, at ~77 Ma, 206 ± 7 Ma, 236 ± 9 Ma, and 261 ± 14 Ma (Figure 7c), are in accordance with those estimated from larger data sets (Figures 7a and 7b).

As expected from the age distribution shown in Figure 6d, the PDP for sample JT1102 yields a significant age mode at 205 ± 7 Ma ($n = 11$). Importantly, while this sample plays a prominent role in the Late Triassic age mode defined for the whole data set, comparison of Figures 7a, 7b, and 7d clearly highlights that the latter age cluster is also found in all other samples from the area, including the syntectonic sandstone. The only specimens that do not record this age are sample JT1106, which was located in the most proximal position, and sample MB136, which underwent extensive Alpine resetting (see discussion in section 5.1.4).

Together, probability density plots and age populations extracted by the unmix ages algorithm converge toward a coherent picture as to the main age ZHe populations, where two main age peaks are identified in the Late Permian (>260 Ma) and toward the Triassic-Jurassic boundary, at 215–200 Ma. A continuous scatter of ages between these two prominent peaks is observed, yielding variable age modes depending on the specific subset under consideration. As discussed in the next section, this variability is most likely resulting from different extents of resetting of Late Permian ages at circa 215–200 Ma. A second-order age population was also detected at circa 177 ± 6 Ma, resting predominantly on detrital zircons from the syntectonic sandstone. Furthermore, a younger age mode was detected at circa 76 Ma. The geological significance of these age modes will be discussed in the following sections, combining the PDP results with considerations on individual samples, in the context of their paleogeographic position.

5.1.2. Late Triassic Heating-Cooling Cycle

The upper crustal Permian magmatic rocks show a systematic younging trend from east to west, with the dominant ZHe age population ranging from circa 280 Ma in the proximal to circa 215–200 Ma in the relatively more distal part of the rifted margin (Figure 6).

For the most proximal sample, a Permian ignimbrite collected about 50 km to the NE of the Sostegno Basin (JT1106), in the western part of the Lombardian Basin, the primary ZHe population clusters tightly at 288–280 Ma. Considering that the emplacement age of the volcanic complex in the same locality is bracketed to the 298–281 Ma interval [*Schaltegger and Brack*, 2007], our ZHe ages record primary postmagmatic cooling. The unimodal distribution of Permian ZHe ages and the lack of any age correlation with Ue strongly suggest that following rapid cooling in the early Permian, this sample resided at $T \ll 140°$ throughout the rest of its geological evolution. A proximal sample immediately to the west of the Lombardian Basin (JT1105) is characterized by somewhat scattered ZHe ages, whereby ages falling within the known effusion interval are rare, whereas a main age cluster at circa 250–255 Ma is detected. Furthermore, a significant ZHe age spread down to ~210 Ma is detected, hinting at minor rift-related post-210 Ma resetting.

The younging trend detected in sample JT1105 becomes significantly more apparent moving westward, underneath the Sostegno Basin, where sample JT 1103 (1.4–1.5 km of overburden; Table 1) exhibits a complex ZHe age spectrum with both Permian and Triassic ages. While the older ZHe ages, at circa 260 Ma, are similar to proximal margin samples (JT1105/JT1106), the younger Triassic population is spread out in the 230–200 Ma interval, suggesting partial resetting. This trend is further corroborated by sample JT1102 (2.6–2.7 km of overburden), where no Permian ZHe ages are preserved any longer and the single dominant Late Triassic age population is found. The lack of any positive age correlation with Ue for these Triassic ZHe ages indicates that this sample cooled from temperatures >180°C in Late Triassic times. Considering that in the Late Triassic this sample rested underneath <3000 m of overburden (Table 1), where significantly lower temperatures would be expected in the context of "normal" thermal gradients of approximately 30°C/km, our data set is indicative of cooling following episodic heating. Indeed, while the Late Triassic age population is most evident in sample JT1102, all other samples from the Sostegno-Fenera area, including the locally sourced syntectonic sandstone, provided zircons with ZHe ages in the 210–200 Ma range (Figure 7).

It should be noted that the Upper Triassic age population cannot result from partial He loss during the Alpine orogeny, as (1) the Fenera Basin, cropping out between samples JT1103 and JT1105, never experienced temperatures in excess of 60–70°C [*Fantoni and Scotti*, 2003]; (2) no Alpine resetting of ZHe ages is observed in the San Quirico sandstone from the Sostegno Basin, directly next to samples JT1102 and JT1103; and (3) in the most reset sample (JT1102) similar ages in the 215–200 Ma interval are measured from zircons with widely different Ue contents. In the latter sample, partial Alpine resetting is observed only for zircons with Ue > 850 ppm, which are known to be characterized by markedly lower retentivity [e.g., *Guenthner et al.,* 2014].

When put into their proper Triassic paleodepth and paleogeographic framework, the E-W age trend emerging from the regional ZHe study presented here provides key insights on the rift-related Triassic thermal structure of the western end of the Adriatic microplate. Most importantly, samples from similar upper crustal levels with Permian protolith cooling ages across the Adriatic margin show a dramatic increase in Late Triassic paleotemperatures toward the future distal part of the margin over a horizontal distance of a few tens of kilometers (Figure 7). This temperature increase is best visualized considering the most easterly and westerly located samples: a proximal sample (JT1106) that, by the end of the Triassic, resided underneath approximately 3000–3500 m of overburden did not record any rift-related He loss; on the other hand, a sample located in a more westerly position, residing underneath $<$3000 m of overburden, recorded complete He loss in the Late Triassic, indicative of ambient temperatures $>$180°C. As pointed out previously, samples located in intermediate positions and/or shallower paleodepths underwent partial He loss in the Late Triassic. The age invariance and lack of correlation with Ue or grain size from sample JT1102 indicates that temperatures $>$180°C were likely very short lived and that rapid cooling to $T < 140$°C was attained in latest Triassic to earliest Jurassic times.

Although we are aware that the thermochronological evidence provided here for this heating-cooling cycle originated from a relatively small area, it is important to note that the occurrence, preservation, and detection of rift-related thermal spikes rest on access to rock specimens that (1) were part of paleogeographically distal domains, (2) resided at sufficient paleodepths for suitable thermochronometers to record resetting, and (3) underwent very limited orogenic thermal overprint. These criteria are likely to be met only very rarely in fossil rifted margins, which are stacked in orogenic belts, especially considering that deformation is normally partitioned preferentially along hyperextended margins during inversion [*Lundin and Doré,* 2011; *Beltrando et al.,* 2014; *Tugend et al.,* 2014].

5.1.3. Synextensional Detrital Zircon (U-Th)/He Ages

Detrital samples from Late Pliensbachian to Toarcian age strata [*Berra et al.,* 2009] in the Fenera and Sostegno Basins yield ages equal to or older than their corresponding depositional ages and thus appear to preserve the original detrital age distribution. This notion is also supported by estimated maximum burial temperatures of $<$60–70°C for the base of the Fenera Basin [*Fantoni and Scotti*, 2003]. The samples from the Fenera Basin (MB1238 and MB1239) show a detrital ZHe age spectrum (~270 Ma to circa 170 Ma), spanning components comparable to cooling ages estimated in the upper crust of the proximal margin (modes at circa 250 Ma), to Late Triassic cooling ages (mode at circa 207 Ma), to syndepositional Pliensbachian-Toarcian ages (youngest ages at 171 ± 14 Ma). Nearly identical detrital signatures are exhibited by a sample from the Sostegno Basin (MB1237), which records detrital ZHe ages ranging from circa 300 Ma to circa 177 ± 14 Ma. Therefore, the detrital ZHe ages from the synrift sandstone record progressive unroofing of the Adriatic margin, with cooling ages that are alternatively (1) prerift, (2) partially to totally reset during the Triassic heat pulse, or (3) Early Jurassic. The youngest ZHe ages demonstrate the synrift character of the Late Pliensbachian-Toarcian samples from the Sostegno and Fenera Basins amid the presence of zero lag time ZHe ages (i.e., youngest cooling ages = depositional ages). Therefore, the ZHe age distribution in the San Quirico sandstone, combined with the biostratigraphic constraints on their deposition, indicates that significant unroofing was accomplished in the area through the activity of normal faults in the Late Pliensbachian to Toarcian. Considering that the youngest detrital ZHe ages are significantly younger than the ZHe ages (215–200 Ma) of the underlying Permian basement, the rift-related tectonic unroofing in this part of the margin postdated the Late Triassic heating-cooling cycle.

5.1.4. Cretaceous Zircon (U-Th)/He Ages

As shown in section 4, post-Jurassic ZHe ages were measured in five samples and post-Jurassic age modes are apparent in probability density plots (Figure 7). As discussed in section 5.1.1, only the age mode at 76 Ma ($n = 8$) is considered as geologically meaningful, while the older mode at 126–127 Ma ($n = 11$) is considered spurious and the single age at 43 Ma is ignored in the following discussion.

MB1236 and JT1106, which were collected at either ends of the transect investigated here (Figure 2) and were placed at the greatest depth within the Mesozoic margin (Table 1), yielded the majority of post-Jurassic ages (Figure 6 and Table 2). The westernmost sample, MB1236, shows a discernible age-Ue correlation, as the youngest and oldest ZHe ages, at 72 ± 4 Ma and 180 ± 11 Ma, were estimated from the crystals yielding the highest and lowest Ue, respectively. This age-Ue relationship is indicative of partial diffusive resetting of the whole zircon crystal population through episodic reheating, for which a maximum age of 72 ± 4 Ma

can be proposed. Partial resetting of Permian ages is also relatively common in JT1106, where no clear age-Ue correlation exists and a ZHe age population falls in the 82–74 Ma interval. In the remaining samples, Cretaceous ages are found only in a handful of zircons, including crystals with Ue > 850 from JT1102 and one crystal from sample MB1238, characterized by the highest Ue (680 ppm). Furthermore, an age cluster at circa 80 Ma is observed in sample JT1103, where no clear age-Ue correlation is apparent.

Therefore, the youngest post-Jurassic age mode determined for the entire data set at 76 Ma is interpreted as recording complete resetting of individual crystals during the Alpine orogeny. Resetting in the 80–70 Ma interval was probably achieved through conductive, regionally homogeneous reheating at the western end of the study area, where MB1236 and JT1102 display a clear age-Ue correlation. Considering that only zircon crystals with Ue > 850 were reset in JT1102, while all crystals underwent partial resetting in sample MB1236, indicates that the latter resided at higher temperature in the Cretaceous. The implied field gradient is not surprising, as MB1336 is located closer to the Cremosina-Marzio Line and the Periadriatic Line, separating the relatively weakly deformed Southern Alps from the Western Alps, which underwent pervasive deformation/metamorphism during the Cretaceous/Tertiary Alpine orogeny. Therefore, this thermal field gradient is likely related to tectonic burial and reheating in the footwall of major Alpine tectonic structures. In all other samples, the paucity of reset zircons, coupled with a lack of age-Ue correlation, is considered as indicative of nonconductive resetting, possibly through fracture-driven influx of hot fluids during Alpine deformation. Notably, the circa 79 Ma age cluster recorded by sample JT1106 might be related to the well-documented low-T long-wavelength folding of the Permian-Mesozoic volcano-sedimentary cover in the Campo dei Fiori Basin, immediately to the SE of the Cremosina-Marzio fault system [*Casati*, 1978]. Therefore, the post-Jurassic ages are attributed to resetting during the Alpine orogeny, increasing toward the Cremosina-Marzio fault system. The 80–70 Ma interval is considered as the best estimate for the timing of this resetting, while the few older ages are attributed to partial resetting of the older age populations found in each sample.

The existing constraints on the timing of the onset of Alpine deformation in the Southern Alps, albeit rare, are consistent with the results arising from this study. The pre-Adamello fold and thrust belt [e.g., *Castellarin et al.,* 2006], which resulted from stacking of predominantly basement nappes originally located underneath the Lombardian Basin, has been constrained to the Late Cretaceous, based on biostratigraphic ages of the Cretaceous flysch [*Bersezio et al.,* 1993] and on $^{40}Ar/^{39}Ar$ dating at 80–68 Ma of pseudotachylites found along the Porcile thrust (Figure 2a) [*Meier*, 2003; *Zanchetta et al.,* 2011]. Furthermore, the onset of Alpine metamorphism at anchizonal conditions along the Internal Canavese Line, at the western end of the Southern Alps, has been dated at circa 75 Ma by K-Ar geochronology [*Zingg et al.,* 1976]. These estimates for low-grade Alpine deformation are consistent with the more extensively studied early stages of Alpine metamorphism in the Western Alps, where the distalmost part of the Adriatic margin underwent multistage metamorphism at HP conditions in the 85–70 Ma interval [*Rubatto et al.,* 2011; *Regis et al.,* 2014].

5.2. Reconciling Thermal Evolution and Deformation History at the Western End of the Southern Alps

The newly determined tectonothermal evolution of the upper crustal rocks from the western edge of the Adriatic microplate can be combined with the existing constraints on the tectonostratigraphic history (Figure 3) (*Bertotti et al.* [1993], *Berra et al.* [2009], and *Gaetani* [2010] for detailed reviews) and with the tectonometamorphic evolution of the Ivrea Zone (Figure 8). This approach provides an unprecedented view at the evolving crustal architecture and thermal structure along the western edge of the Adriatic microplate, as well as allowing potential insights on the processes responsible for rift localization. The evolutionary model presented here (Figure 9) integrates the results from this study as well as from recent investigations of the Canavese Zone [*Ferrando et al.,* 2004; *Beltrando et al.,* 2015] and Ivrea Zone [*Ewing et al.,* 2013, 2015; *Zanetti et al.,* 2013; *Smye and Stockli*, 2014; *Schaltegger et al.,* 2015] into the original model proposed by *Bertotti et al.* [1993] for the Lombardian Basin and CBC area. The following discussion is focused on the Late Norian to Middle Jurassic evolution, which unfolded onto the previously established Anisian-Carnian architecture of the northern end of the Adriatic microplate (Figure 9a).

5.2.1. The Adriatic Crust at 220–200 Ma

As argued in section 5.1.2, the age cluster at 215–200 Ma measured both from basement samples and in detrital zircons from synrift deposits is best explained as resulting from episodic short-lived heating-cooling

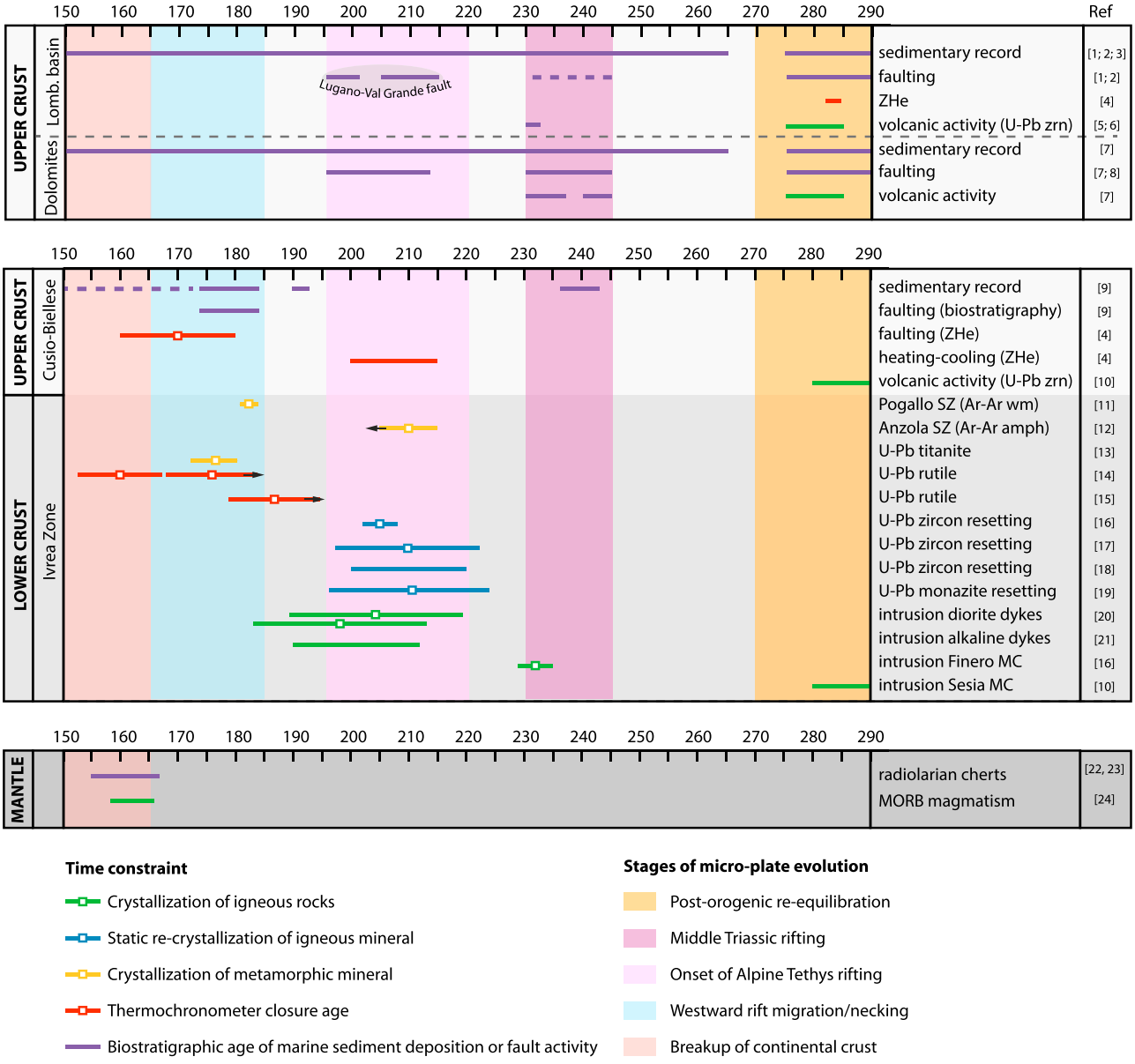

Figure 8. Summary table of selected biostratigraphic, geochronological, and thermochronological data related to the evolution of the western end of the Adriatic margin, now sampled in the Cusio-Biellese-Canavese area (CBC) and in the Ivrea Zone. Key aspects of the evolution of the Lombardian Basin, Dolomites, and subcontinental mantle are also reported. Arrows are used when the specific technique provided only minimum or maximum ages (see discussion in the text). References: (1) *Bertotti* [1991], (2) *Bertotti et al.* [1993], (3) *Berra and Carminati* [2010], (4) this study, (5) *Schaltegger and Brack* [2007], (6) *Cassinis et al.* [2008], (7) *Gaetani* [2010], (8) *Doglioni* [1987], (9) *Berra et al.* [2009], (10) *Quick et al.* [2009], (11) *Mulch et al.* [2002b], (12) *Brodie et al.* [1989], (13) *Mulch et al.* [2002a], (14) *Ewing et al.* [2015], (15) *Smye and Stockli* [2014], (16) *Zanetti et al.* [2013], (17) *Vavra et al.* [1999], (18) *Ewing et al.* [2013], (19) *Vavra and Schaltegger* [1999], (20) *Mazzucchelli et al.* [2010], (21) *Schaltegger et al.* [2015], (22) *Bill et al.* [2001], (23) *Cordey et al.* [2012]; and (24) *Li et al.* [2013].

of the Cusio-Biellese area in the uppermost Triassic. It is worth stressing that no evidence for a similar heating-cooling cycle was found in more easterly located areas, while the Alpine thermal overprint prevents investigating the existence of a similar T history farther to the west, in the Canavese Zone.

However, several additional lines of evidence suggest that the heating-cooling cycle detected in the Cusio-Biellese area is related to regional-scale tectonic processes (Figures 8 and 9b). As extensively discussed in section 2.2, U-Pb geochronology from the Ivrea-Verbano Zone, now located immediately to the west of the Cusio-Biellese area (Figure 2), repeatedly provided evidence for hot fluid circulation at lower crustal depth during the uppermost Triassic. Additionally, widespread resetting of U-Pb geochronometers was coeval with

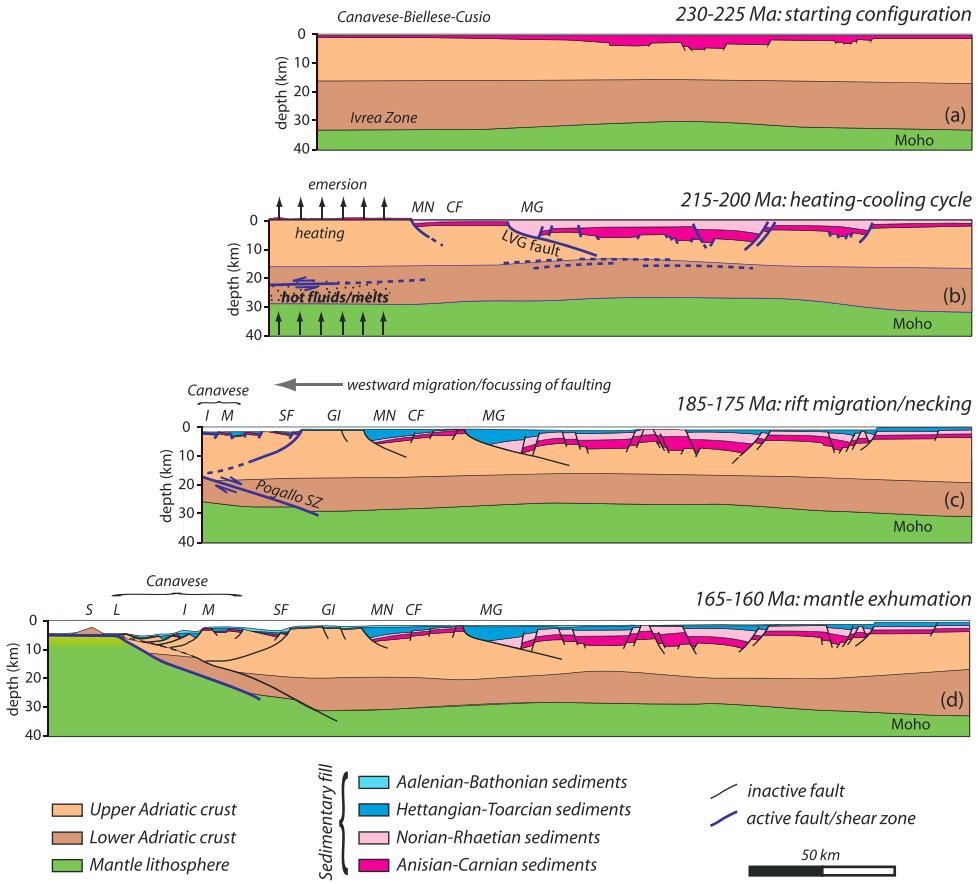

Figure 9. Conceptual model of the tectonothermal evolution of the Southern Alps in the Middle Triassic-Middle Jurassic interval. The evolution of the Lombardian Basin and Dolomites is from *Bertotti et al.* [1993]. MG: Monte Generoso Basin; CF: Campo dei Fiori Basin; MN: Monte Nudo Basin; GI: Gozzano-Invorio; SF: Sostegno-Fenera Basins; M: Montalto area (Canavese Zone); I: Issiglio area (Canavese Zone); L: Levone area (Canavese Zone); and S: Sesia Zone.

(rare) magmatism, reported both from the northern and southern ends of the Ivrea Zone [*Mazzucchelli et al.,* 2010; *Schaltegger et al.,* 2015].

Fluid-driven heat advection along the future distal part of the Adriatic margin provides a viable mechanism to account for the high temperatures locally attained at shallow crustal levels in the Cusio-Biellese area, too. Heat transfer by convection has the ability to result in anomalously high temperatures at shallow crustal depths, partly unrelated to the crustal-scale thermal gradient. Although future work will be necessary to document fluid flux at shallow crustal levels within the Southern Alps, this latter hypothesis is favored on the ground that regional-scale fluid flow at lower crustal depths in the 212–190 Ma interval has already been proposed to account for several features of the Ivrea Zone evolution [*Schaltegger et al.,* 2015]. The longer time span of fluid-mediated heat advection in the lower crust with respect to the CBC area might either reflect sample bias or earlier thermal decay at upper crustal levels, after an initial crustal-wide pulse.

Therefore, a crustal-wide thermal anomaly was established in the Late Triassic, possibly at circa 215–210 Ma, within the domain where rifting leading to the formation of the Alpine Tethys was later focused. The onset of this thermal anomaly is coeval with a regional-scale rifting stage recorded both within the Adriatic Plate and along the future European margin of the Alpine Tethys. In the Lombardian Basin, to the east of the CBC area, a thick Norian-Rhaetian sedimentary sequence was deposited in half grabens (Figure 9b). In the Monte Generoso Basin, at the western end of the Lombardian Basin, extension was accommodated by a major east dipping normal fault, labeled Lugano-Val Grande fault, which soled out in the middle crust [*Bertotti et al.,* 1993, 1999]. However, despite the evidence for localized crustal thinning, our data set suggests that the Lombardian Basin was not affected by a heating-cooling cycle comparable to the one detected farther to

the west, in the CBC area. This difference suggests that the CBC area resided in close proximity to the heat source, along the future western edge of the Adriatic Plate.

Despite the lack of evidence for Late Triassic normal faulting in the CBC area, evidence for rift-related ductile shearing in the Ivrea Zone at 210–200 Ma is available from the literature (see discussion in section 2.2), potentially suggesting that upper and lower crustal deformation were decoupled in the early stages of rifting along the future western edge of the Adriatic Plate (Figure 9b).

5.2.2. The Adriatic Crust at 200–170 Ma

Drowning is recorded in several parts of the CBC, starting from the upper Sinemurian (195–190 Ma), possibly as a result of thermal relaxation following the previous heating-cooling cycle. The onset of drowning predated the westward migration and localization of upper crustal deformation, widely documented in the literature [e.g., *Bertotti et al.,* 1993; *Berra et al.,* 2009] and supported by our new data from the syntectonic San Quirico sandstone (Figure 9c). Palynological data from this sandstone suggest an Upper Pliensbachian to Toarcian age of deposition, which is within error with the youngest ZHe ages from detrital zircons from the Sostegno and Fenera Basins, at 177 ± 14 Ma and 171 ± 14 Ma, respectively. Therefore, our new ZHe data from detrital zircons indicate that fault-related denudation was very efficient, considering that the cooling ages overlap with the biostratigraphic age of the sediments (i.e., zero lag time).

Extensional deformation in the Late Pliensbachian to Toarcian was predominantly accommodated along WSW dipping normal faults, bounding newly formed half grabens, while shearing at middle to lower crustal levels was accommodated along the east dipping Pogallo shear zone (Figure 9c). The resulting crustal-scale architecture, whereby thinning is accommodated by outboard dipping faults at upper crustal depth and inboard dipping shear zones at middle to lower crystal depth, is consistent with the CBC-Ivrea Zone pair residing along the necking zone of the Adriatic margin of the Alpine Tethys. Considering the existing geochronological, thermochronological, and biostratigraphic constraints from both domains (Figure 7), necking likely occurred in the 185–175 Ma interval.

5.2.3. The Adriatic Crust at 170–160 Ma

Following crustal necking, farther westward migration of deformation in the Aalenian-Bajocian led to regional exhumation of continental basement at the basin floor, as recorded in several parts of the Canavese Zone [*Ferrando et al.,* 2004] and in the Sesia Zone, located farther to the west [*Beltrando et al.,* 2014]. Regional-scale basement-cover relationships suggest that long-offset detachment faults played a key role in accommodating the latest stages of deformation in either domains. However, relatively poor outcropping conditions in the Canavese Zone [*Beltrando et al.,* 2015] and the pervasive Alpine metamorphic overprint in the Sesia Zone [*Rubatto et al.,* 2011] prevent assessing the lateral extent and role of these brittle structures in accommodating crustal extension. Continued crustal thinning eventually led to mantle exhumation, recorded in the southernmost part of the Canavese Zone (Figure 9d) [*Beltrando et al.,* 2015] and throughout the Alpine Tethys [*Bill et al.,* 2001].

5.3. Rift Localization Triggered by Fluid/Melt Advection to the Crust?

Recent studies in the northern Adriatic margin of the Alpine Tethys preserved in the Swiss Alps provided a well-constrained picture as to the evolving crustal architecture during rift migration and focusing, in the lead up to complete crustal excision along the Alpine Tethys margin [*Müntener and Hermann,* 2001; *Manatschal,* 2004; *Mohn et al.,* 2012]. In the northern Adriatic margin, rift focusing along the future western edge of the microplate followed the onset of ductile shearing at middle crustal depth, starting at circa 205–200 Ma, and was contemporaneous with the activity of large-offset detachment faults at circa 180 Ma [*Mohn et al.,* 2012]. However, in these areas, the Alpine thermal overprint prevents inferences on the rift-related thermal evolution by low-temperature thermochronology.

The southern Adriatic margin discussed here, instead, offers additional insights on the rift-related thermal evolution, thanks to the limited Alpine thermal overprint. The key constraints arising from this study, in combination with published data from the Ivrea Zone, indicate that (1) rift focusing is predated by a crustal-scale thermal anomaly, starting from circa 215–200 Ma and decaying in the 200–190 Ma interval, depending on the crustal depth under consideration, and (2) crustal-scale extensional deformation at lower and upper crustal depths was established no earlier than 185 Ma and culminated in complete crustal excision by circa 165 Ma. The relative timing of the thermal anomaly with respect to the rift localization, as well as the spatial distribution of this anomaly, which is not detected in the more proximal domains, is suggestive of a causative link between the two processes.

At present, relatively limited information is available on the heat transfer mechanisms in the 215–200 Ma interval. Existing data from the Ivrea Zone indicate that reheating of the crustal section was, at least partly, achieved through heat advection by hot fluids and melts, likely related to protracted influx of highly differentiated melts from enriched, lithospheric mantle [*Schaltegger et al.,* 2015]. Indeed, protracted influx of mantle-derived fluids has been well documented in the northern part of the Ivrea Zone [*Giovanardi et al.,* 2014; *Schaltegger et al.,* 2015]. An additional heat source might have been provided by conductive heating in the context of depth-dependent thinning of the lithospheric section, resulting in transient heating of the weakly thinned domains [e.g., *Sandiford and Powell*, 1986]. Indeed, future work along this fossil margin will be necessary to provide tighter constraints on the heat transfer mechanisms that were active in the area at 215–200 Ma.

Despite these uncertainties, existing information from the western end of the Adriatic Plate suggests that thermal softening of the Adriatic crust was an important precursor to rift focusing within the future western edge of the Adriatic Plate. This inference is in line with several preexisting studies, suggesting that episodic thinning on the mantle lithosphere, either by plume activity [e.g., *White*, 1989; *Buiter and Torsvik*, 2014] or by other processes, including thermal incubation of the lithosphere beneath supercontinents [*Coltice et al.,* 2007], may be important precursors both of rift migration and hyperextension.

6. Conclusions

This study provides new insights on the processes responsible for rift localization in a fossil rifted margin belonging to the Adriatic microplate, now sampled in the Italian Southern Alps. In these areas, several stages of extensional faulting spanning the Middle Triassic to the Sinemurian were followed by westward rift migration and focusing in the Late Pliensbachian-Toarcian. Newly acquired ZHe data indicate that the future western edge of the Adriatic microplate, facing the Alpine Tethys oceanic domain, records a localized heating-cooling cycle at 215–200 Ma, coupled with the influx of mantle-derived fluids/melts. This regional thermal perturbation was coeval with the onset of rift-related shearing at lower crustal depths, which predated normal faulting at upper crustal levels by circa 10–15 Myr. Extensional deformation at all crustal levels, recorded starting from circa 185 to 180 Ma, led to the formation of new depocenters at the future western end of the Adriatic Plate, in the lead up to complete crustal excision, achieved at circa 165 Ma. Heat transfer toward shallow crustal levels was likely achieved through a combination of advection of mantle-derived fluids/melt and conduction, in the context of lithospheric-scale depth-dependent thinning.

Acknowledgments

The data for this paper are available by contacting the corresponding author. Fabrizio Berra, Vincenzo Picotti, and Roberto Compagnoni are thanked for discussions. Fabrizio Berra is also thanked for providing Figure 5b. Tanya Ewing provided valuable help with data statistics. The Margin Modelling 3 consortium is gratefully acknowledged for providing financial support for this research. We would also like to acknowledge support from UT's Jackson School of Geosciences for (U-Th)/He analyses and L. Stockli, S. Cooperdock, and N. Seymour for their help with analytical work in the UT Geo- and Thermochronometry Laboratory. Reviews by Philip Ball and editorial comments helped in clarifying several aspects of this study.

References

Ball, P., G. Eagles, C. Ebinger, K. McClay, and J. Totterdell (2013), The spatial and temporal evolution of strain during the separation of Australia and Antarctica, *Geochem. Geophys. Geosyst.*, *14*, 2771–2799, doi:10.1002/ggge.20160.

Beltrando, M., G. Manatschal, G. Mohn, G. V. Dal Piaz, A. Vitale Brovarone, and E. Masini (2014), Recognizing remnants of magma-poor rifted margins in high-pressure orogenic belts: The Alpine case study, *Earth Sci. Rev.*, *131*, 88–115, doi:10.1016/j.earscirev.2014.01.001.

Beltrando, M., R. Compagnoni, S. Ferrando, G. Mohn, G. Frasca, N. Odasso, Z. Vukmanovič, and E. Masini (2015), Crustal thinning and mantle exhumation in the Levone area (Southern Canavese Zone, Western Alps), in *A Field Guide Across the Margins of Alpine Tethys*, *J. Virtual Explor.*, vol. 48, edited by G. Manatschal et al., The Virtual Explorer, Pty. Ltd., Clear Range, Australia, doi:10.3809/jvirtex.2013.00326.

Bernoulli, D. (1964), Zur Geologie des Monte Generoso (Lombardische Alpen), *Beitr. Geol. Karte Schweiz.*, *118*, 1–134.

Berra, F., and E. Carminati (2010), Subsidence history from a backstripping analysis of the Permo-Mesozoic succession of the Central Southern Alps (Northern Italy), *Basin Res.*, *22*, 952–975, doi:10.1111/j.1365-2117.2009.00453.x.

Berra, F., M. T. Galli, F. Reghellin, S. Torricelli, and R. Fantoni (2009), Stratigraphic evolution of the Triassic-Jurassic succession in the Western Southern Alps (Italy): The record of the two-stage rifting on the distal passive margin of Adria, *Basin Res.*, *21*, 335–353, doi:10.1111/j.1365-2117.2008.00384.x.

Bersezio, R., M. Fornaciari, R. Gelati, A. Napolitano, and A. Valdisturlo (1993), The significance of the Upper Cretaceous to Miocene clastic wedges in the deformation history of the Lombardian Southern Alps, *Geol. Alp.*, *69*, 3–20.

Bertotti, G. (1991), Early Mesozoic extension and Alpine shortening in the western Southern Alps: The geology of the area between Lugano and Menaggio (Lombardy, Northern Italy), *Mem. Sci. Geol. Padova*, *43*, 17–123.

Bertotti, G., V. Picotti, D. Bernoulli, and A. Castellarin (1993), From rifting to drifting: Tectonic evolution of the South Alpine upper crust from Triassic to Early Cretaceous, *Sedim. Geol.*, *86*, 53–76.

Bertotti, G., D. Seward, J. Wijbrans, M. ter Voorde, and A. J. Hurford (1999), Crustal thermal regime prior to, during, and after rifting: A geochronological and modeling study of the Mesozoic South Alpine rifted margin, *Tectonics*, *18*, 185–200, doi:10.1029/1998TC900028.

Bigi, G., A. Castellarin, M. Coli, G. V. Dal Piaz, R. Sartori, P. Scandone, and G. B. Vai (1990), Structural model of Italy 1:500.000, sheet 1, C.N.R., Progetto Finalizzato Geodinamica, S.EL.CA., Firenze.

Biino, G., and R. Compagnoni (1989), The Canavese Zone between the Serra d'Ivrea and the Dora Baltea River (Western Alps), *Eclogae Geol. Helv.*, *82*, 413–427.

Bill, M., L. O. O'Dogherty, J. Guex, P. O. Baumgartner, and H. Masson (2001), Radiolarite ages in Alpine-Mediterranean ophiolites: Constraints on the oceanic spreading and the Tethys-Atlantic connection, *Geol. Soc. Am. Bull.*, *113*, 129–143.

Bonadiman, C., M. Coltorti, and F. Siena (1994), Petrogenesis and T-fO2 estimates of Mt. Monzoni complex (Central Dolomites, Southern Alps): A Triassic shoshonitic intrusion in a transcurrent geodynamic setting, *Eur. J. Mineral.*, *6*, 943–966.

Boriani, A. C., and I. M. Villa (1997), Geochronology of regional metamorphism in the Ivrea-Verbano Zone and Serie dei Laghi, Italian Alps, *Schweiz. Mineral. Petrogr. Mitt.*, *77*, 381–401.

Boriani, A., and E. Giobbi (2004), Does the basement of western Southern Alps display a tilted section through the continental crust? A review and discussion, *Per. Mineral.*, *73*, 5–22.

Boriani, A., and R. Sacchi (1973), Geology of the junction between the Ivrea–Verbano and Strona–Ceneri Zones (southern Alps), *Mem. Ist. Geol. Min. Univ. Padova*, *28*, 1–36.

Boriani, A., E. Origoni Giobbi, A. Borghi, and V. Caironi (1990), The evolution of the "Serie dei Laghi" (Strona-Ceneri and Schisti dei Laghi): The upper component of the Ivrea-Verbano crustal section, Southern Alps, North Italy and Ticino, Switzerland, *Tectonophysics*, *182*, 103–118.

Bosworth, W., P. Huchon, and K. McClay (2005), The Red Sea and Gulf of Aden Basins, *J. Afr. Earth Sci.*, *43*, 354–378.

Brodie, K. H., D. Rex, and E. H. Rutter (1989), On the age of deep crustal extensional faulting in the Ivrea Zone, Northern Italy, Alpine tectonics, *Geol. Soc. Spec. Publ.*, *45*, 203–210.

Buiter, S. J. H., and T. H. Torsvik (2014), A review of Wilson Cycle plate margins: A role for mantle plumes in continental break-up along sutures?, *Gondwana Res.*, *26*, 627–653.

Bütler, E., W. Winkler, and M. Guillong (2011), Laser ablation U/Pb age patterns of detrital zircons in the Late Maastrichtian–Early Eocene Schlieren Flysch (Central Switzerland): New proves on the detrital sources, *Swiss J. Geosci.*, *104*, 225–236.

Carraro, F., and L. Fiora (1974), Studio petrografico e stratigrafico delle tufiti mediotriassiche dei lembi di Crevacuore e di Sostegno, *Riv. ital. Paleontologia*, *80*, 167–192.

Carraro, F., G. Bortolami, and R. Sacchi (1967), Carta Geologica d'Italia 1/100000, sheet 43, Servizio Geologico d'Italia.

Casati, P. (1978), Tettonismo e sedimentazione nel settore occidentale delle Alpi Meridionali durante il tardo Paleozoico, il Triassico e il Giurassico, *Riv. ital. Paleontologia Stratigrafia*, *84*, 313–326.

Cassinis, G., and U. Zezza (1982), Dati geologici e petrografici sui prodotti del magmatismo triassico delle Prealpi Bresciane, in *Guida Alla Geologia del Sudalpino Centro-Orientale*, edited by A. Castellarin and G. B. Vai, pp. 157–171, Bologna, Guide Reg. Soc. Geol. It.

Cassinis, G., L. Cortesogno, L. Gaggero, C. R. Perotti, and L. Buzzi (2008), Permian to Triassic geodynamic and magmatic evolution of the Brescian Prealps (eastern Lombardy, Italy), *Boll. Soc. Geol. Ital.*, *127*, 501–518.

Cassinis, G., C. R. Perotti, and A. Ronchi (2012), Permian continental basins in the Southern Alps (Italy) and peri-Mediterranean correlations, *Int. J. Earth Sci.*, *101*, 129–157.

Castellarin, A., G. B. Vai, and L. Cantelli (2006), The Alpine evolution of the Southern Alps around the Giudicarie faults: A Late Cretaceous to Early Eocene transfer zone, *Tectonophysics*, *414*, 203–223, doi:10.1016/j.tecto.2005.10.019.

Cohen, K. M., S. C. Finney, P. L. Gibbard, and J.-X. Fan (2013), The ICS international chronostratigraphic chart, *Episodes*, *36*, 199–204 updated in 2015.

Coltice, N., B. R. Phillips, H. Bertrand, Y. Ricard, and P. Rey (2007), Global warming of the mantle at the origin of flood basalts over supercontinents, *Geology*, *35*, 391–394, doi:10.1130/G23240A.

Cordey, F., P. Tricart, S. Guillot, and S. Schwartz (2012), Dating the Tethyan Ocean in the Western Alps with radiolarite pebbles from synorogenic Oligocene molasse basins (southeast France), *Swiss J. Geosci.*, doi:10.1007/s00015-012-0090-8.

Cowie, P. A., J. R. Underhill, M. D. Behn, J. Lin, and C. E. Gill (2005), Spatio-temporal evolution of strain accumulation derived from multi-scale observations of Late Jurassic rifting in the northern North Sea: A critical test of models for lithospheric extension, *Earth Planet. Sci. Lett.*, *234*, 401–419, doi:10.1016/j.epsl.2005.01.039.

D'Adda, P., A. Zanchi, M. Bergomi, F. Berra, M. Malusà, A. Tunesi, and S. Zanchetta (2011), Polyphase thrusting and dyke emplacement in the central Southern Alps (Northern Italy), *Int. J. Earth Sci.*, *100*, 1095–1113, doi:10.1007/s00531-010-0586-2.

Decarlis, A., G. Dallagiovanna, A. Lualdi, M. Maino, and S. Seno (2013), Stratigraphic evolution in the Ligurian Alps between Variscan heritages and the Alpine Tethys opening: A review, *Earth Sci. Rev.*, *125*, 43–68, doi:10.1016/j.earscirev.2013.07.001.

Demarchi, G., J. Quick, S. Sinigoi, and A. Mayer (1998), Pressure gradient and original orientation of a lower-crustal intrusion in the Ivrea-Verbano Zone, Northern Italy, *J. Geol.*, *106*, 609–621.

Desio, A. (1973), Geologia dell'Italia, XXXV-1 081, UTET, Torino, 244 pp.

Direen, N. G., I. Borissova, H. M. J. Stagg, J. B. Colwell, and P. A. Symonds (2007), Nature of the continent–ocean transition zone along the southern Australian continental margin: A comparison of the Naturaliste Plateau, south-western Australia, and the central Great Australian Bight sectors, in *Imaging, Mapping and Modelling Continental Lithosphere Extension and Breakup*, edited by G. D. Karner, G. Manatschal, and L. M. Pinheiro, *Geol. Soc. London Spec. Publ.*, *282*, 235–261.

Doglioni, C. (1987), Tectonics of the Dolomites (Southern Alps, Northern Italy), *J. Struct. Geol.*, *9*, 181–193.

Elter, G., P. Elter, C. Sturani, and M. Weidmann (1966), Sur la prolongation du domaine ligure de l'Apennin dans le Monferrat et les Alpes et sur l'origine de la Nappe de la Simme s.l. des Préalpes romandes et chablaisiennes, *Arch. Sci. (Genève)*, *19*, 279–377.

Ewing, T. A., J. Hermann, and D. Rubatto (2013), The robustness of the Zr-in-rutile and Ti-in zircon thermometers during high-temperature metamorphism (Ivrea–Verbano Zone, Northern Italy), *Contrib. Mineral. Petrol.*, *4*, 757–779, doi:10.1007/s00410-012-0834-5.

Ewing, T. A., D. Rubatto, M. Beltrando, and J. Hermann (2015), Constraints on the thermal evolution of the Adriatic margin during Jurassic continental break-up: U–Pb dating of rutile from the Ivrea–Verbano Zone, Italy, *Contrib. Mineral. Petrol.*, *169*, doi:10.1007/s00410-015-1135-6.

Faleide, J. I., F. Tsikalas, A. J. Breivik, R. Mjelde, O. Ritzmann, Ø. Engen, J. Wilson, and O. Eldholm (2008), Structure and evolution of the continental margin off Norway and the Barents Sea, *Episodes*, *31*, 82–91.

Fantoni, R., and P. Scotti (2003), Thermal record of the Mesozoic extensional tectonics in the Southern Alps, *Atti Ticin. Sci. Terra*, *9*, 96–101.

Fantoni, R., A. Decarlis, and E. Fantoni (2003), L'estensione mesozoica al margine occidentale delle Alpi Meridionali, *Atti Ticin. Sci. Terra*, *44*, 97–110.

Farley, K. A., R. A. Wolf, and L. T. Silver (1996), The effects of long alpha-stopping distances on (U-Th)/He ages, *Geochim. et Cosmochim. Acta*, *60*, 4223–4229, doi:10.1016/S0016-7037(96)00193-7.

Ferrando, S., D. Bernoulli, and R. Compagnoni (2004), The Canavese Zone (internal Western Alps): A distal margin of Adria, *Schweiz. Mineral Petrogr. Mitt.*, *84*, 237–256.

Franz, L., and R. L. Romer (2007), Caledonian high-pressure metamorphism in the Strona-Ceneri Zone (Southern Alps of southern Switzerland and Northern Italy), *Swiss J. Geosci.*, *100*, 457–467, doi:10.1007/s00015-007-1232-2.

Gaetani, M. (2010), From Permian to Cretaceous: Adria as pivotal between extensions and rotations of Tethys and Atlantic Oceans, in *The Geology of Italy: Tectonics and Life Along Plate Margins, J. Virtual Explor.*, vol. 36, edited by M. Beltrando et al., The Virtual Explorer, Pty. Ltd., Clear Range, Australia, doi:10.3809/jvirtex.2010.00235.

Garzanti, E., M. Gnaccolini, and F. Jadoul (1995), Anatomy of a semiarid coastal system: The Upper Carnian of Lombardy (Italy), *Riv. It. Paleont. Stratigr.*, *101*, 17–36.
Giovanardi, T., M. Mazzucchelli, A. Zanetti, A. Langone, M. Tiepolo, and A. Cipriani (2014), Occurrence of phlogopite in the Finero Mafic layered complex, *Cent. Eur. J. Geosci.*, *6*, 588–613, doi:10.2478/s13533-012-0186-8.
Gouiza, M., G. Bertotti, M. Hafid, and S. Cloething (2010), Kinematic and thermal evolution of the Moroccan rifted continental margin: Doukkala-High Atlas transect, *Tectonics*, *29*, TC5008, doi:10.1029/2009TC002464.
Govers, R., and R. M. J. Wortel (1993), Initiation of asymmetric extension in continental lithosphere, *Tectonophysics*, *223*, 75–96.
Govi, M. (1977), Carta geologica del distretto vulcanico ad oriente della bassa Valsesia: Pavia, Italy, Centro studi problemi dell'orogeno delle Alpi Occidentali, Consiglio Nazionale delle Ricerche.
Guenthner, W. R., P. W. Reiners, and Y. Tian (2014), Interpreting date–eU correlations in zircon (U-Th)/He datasets: A case study from the Longmen Shan, China, *Earth Planet. Sci. Lett.*, *403*, 328–339.
Handy, M. R. (1987), The structure, age and kinematics of the Pogallo fault zone: Southern Alps, northwestern Italy, *Eclogae Geol. Helv.*, *80*, 593–632.
Handy, M. R., L. Franz, F. Heller, B. Jannot, and R. Zurbroggen (1999), Multistage accretion and exhumation of the continental crust (Ivrea crustal section, Italy and Switzerland), *Tectonics*, *18*, 1154–1177, doi:10.1029/1999TC900034.
Henk, A., L. Franz, S. Teufel, and O. Oncken (1997), Magmatic underplating, extension, and crustal reequilibration: Insights from a cross-section through the Ivrea Zone and Strona-Ceneri Zone, Northern Italy, *J. Geol.*, *105*, 367–377.
Jadoul, F., F. Berra, and S. Frisia (1992), Stratigraphy and paleogeographic evolution of a carbonate platform in an extensional tectonic regime: The example of the Dolomia Principale in Lombardy (Italy), *Riv. It. Paleont. Stratigr.*, *98*, 29–44.
Klötzli, U. S., S. Sinigoi, J. E. Quick, G. Demarchi, C. C. G. Tassinari, K. Sato, and Z. Günes (2014), Duration of igneous activity in the Sesia Magmatic System and implications for high-temperature metamorphism in the Ivrea-Verbano deep crust, *Lithos*, *206–207*, 19–33.
Kozur, H. (1991), The evolution of the Meliata-Hallstatt ocean and its significance for the early evolution of the Eastern Alps and Western Carpathians, *Palaeogeogr. Palaeoclimatol. Palaeoecol.*, *87*, 109–135.
Kusznir, N. J., and R. G. Park (1987), The extensional strength of the continental lithosphere: Its dependence on geothermal gradient, crustal composition and thickness, in *Continental Extensional Tectonics*, *Geol. Soc. London Spec. Publ.*, 26, 35–52.
Li, X. H., M. Faure, W. Lin, and G. Manatschal (2013), New isotopic constraints on age and magma genesis of an embryonic oceanic crust: The Chenaillet Ophiolite in the Western Alps, *Lithos*, *160–161*, 283–291.
Ludwig, K. R. (2003), User's manual for Isoplot 3.00: A geochronological toolkit for Microsoft Excel, Berkeley Geochronology Center Spec. Publ. 4.
Lundin, E. R., and A. G. Doré (2011), Hyperextension, serpentinization, and weakening: A new paradigm for rifted margin compressional deformation, *Geology*, *39*, 347–350, doi:10.1130/G31499.1.
Manatschal, G. (2004), New models for evolution of magma-poor rifted margins based on a review of data and concepts from West Iberia and the Alps, *Int. J. Earth Sci. (Geol. Rundsch.)*, *93*, 432–466.
Manatschal, G., L. Lavier, and P. Chenin (2015), The role of inheritance in structuring hyperextended rift systems: Some considerations based on observations and numerical modeling, *Gondwana Res.*, *27*, 140–164.
Mazzucchelli, M., A. Zanetti, G. Rivalenti, R. Vannucci, C. T. Correia, and C. C. G. Tassinari (2010), Age and geochemistry of mantle peridotites and diorite dykes from the Baldissero body: Insights into the Paleozoic-Mesozoic evolution of the Southern Alps, *Lithos*, *119*, 485–500.
Meier, A. (2003), The periadriatic fault system in Valtellina (N-Italy) and the evolution of the southwestern segment of the Eastern Alps, PhD thesis, ETH Zürich, Zürich, Switzerland.
Mohn, G., G. Manatschal, M. Beltrando, E. Masini, and N. Kusznir (2012), Necking of continental crust in magma-poor rifted margins: Evidence from the fossil Alpine Tethys margins, *Tectonics*, *31*, TC1012, doi:10.1029/2011TC002961.
Montanari, L. (1969), Aspetti geologici del Lias di Gozzano (Lago d'Orta), *Mem. Soc. It. Sc. Nat. Mus. Civico Storia Nat. Milano*, *18*, 25–94.
Mulch, A., M. Rosenau, W. Dorr, and M. R. Handy (2002a), The age and structure of dikes along the tectonic contact of the Ivrea-Verbano and Strona-Ceneri Zones (southern Alps, Northern Italy, Switzerland), *Schweiz. Mineral. Petrogr. Mitt*, *82*, 55–76.
Mulch, A., M. A. Cosca, and M. R. Handy (2002b), In-situ UV-laser $^{40}Ar/^{39}Ar$ geochronology of a micaceous mylonite: An example of defect-enhanced argon loss, *Contrib. Mineral. Petrol.*, *142*, 738–752, doi:10.1007/s00410-001-0325-6.
Müntener, O., and J. Hermann (2001), The role of lower crust and continental upper mantle during formation of non-volcanic passive margins: Evidence from the Alps, in *Non-Volcanic Rifting of Continental Margins: A Comparison of Evidence From Land and Sea*, edited by R. C. L. Wilson et al., *Geol. Soc. London Spec. Publ.*, *187*, 267–288, doi:10.1144/GSL.SP.2001.187.01.13.
Pereira, R., and T. M. Alves (2011), Margin segmentation prior to continental break-up: A seismic–stratigraphic record of multiphased rifting in the North Atlantic (Southwest Iberia), *Tectonophysics*, *505*, 17–34, doi:10.1016/j.tecto.2011.03.011.
Picotti, V., and G. A. Pini (1988), Tettonica sinsedimentaria norica nel settore compreso fra il Lago d'Idro ed il Lago di Garda, *Rend. Soc. Geol. It.*, *11*, 225–230.
Quick, J. E., S. Sinigoi, G. Peressini, G. Demarchi, J. L. Wooden, and A. Sbisà (2009), Magmatic plumbing of a large Permian caldera exposed to a depth of 25 km, *Geology*, *37*, 603–606, doi:10.1130/G30003A.1.
Regis, D., D. Rubatto, J. Darling, B. Cenki-Tok, M. Zucali, and M. Engi (2014), Multiple metamorphic stages within an eclogite-facies terrane (Sesia Zone,Western Alps) revealed by Th-U-Pb petrochronology, *J. Petrol.*, *55*, 1429–1456, doi:10.1093/petrology/egu029.
Rubatto, D., D. Regis, J. Hermann, K. Boston, M. Engi, M. Beltrando, and S. R. B. McAlpine (2011), Yo-yo subduction recorded by accessory minerals in the Italian Western Alps, *Nat. Geosci.*, *4*, 338–342, doi:10.1038/ngeo1124.
Rutter, E. H., K. H. Brodie, and P. Evans (1993), Structural geometry, lower crustal magmatic underplating and lithospheric stretching in the Ivrea-Verbano zone, N. Italy, *J. Struct. Geol.*, *15*, 647–662.
Rutter, E. H., K. Brodie, T. James, and L. Burlini (2007), Large-scale folding in the upper part of the Ivrea-Verbano zone, NW Italy, *J. Struct. Geol.*, *29*, 1–17.
Sambridge, M. S., and W. Compston (1994), Mixture modeling of multicomponent data sets with application to ion-probe zircon ages, *Earth Planet. Sci. Lett.*, *128*, 373–390.
Sandiford, M., and R. Powell (1986), Deep crustal metamorphism during continental extension: Modern and ancient examples, *Earth Planet. Sci. Lett.*, *79*, 151–158.
Schaltegger, U., and P. Brack (2007), Crustal-scale magmatic system during intracontinental strike-slip tectonics: U, Pb and Hf isotopic constraints from Permian magmatic rocks of the Southern Alps, *Int. J. Earth Sci.*, *96*, 1131–1151.
Schaltegger, U., A. Ulianov, O. Müntener, M. Ovtcharova, P. Vonlanthen, T. Vennemann, M. Antognini, and F. Girlanda (2015), Megacrystic zircon with planar fractures in miaskite-type nepheline pegmatites formed at high pressures in the lower crust (Ivrea Zone, Southern Alps, Switzerland), *Am. Mineral.*, *100*, 83–94, doi:10.2138/am-2015-4773.

Schettino, A., and E. Turco (2011), Tectonic history of the western Tethys since the Late Triassic, *Geol. Soc. Am. Bull.*, *123*, 89–105, doi:10.1130/B30064.1.

Schmid, S. M., A. Zingg, and M. Handy (1987), The kinematics of movements along the Insubric Line and the emplacement of the Ivrea Body, *Tectonophysics*, *135*, 47–66.

Schreiber, D., J. M. Lardeaux, G. Martelet, G. Courrioux, and A. Guillen (2010), 3-D modelling of Alpine Mohos in Southwestern Alps, *Geophys. J. Int.*, *180*, 961–975, doi:10.1111/j.1365-246X.2009.04486.x.

Siegesmund, S., P. Layer, I. Dunkl, A. Vollbrecht, A. Steenken, K. Wemmer, and H. Ahrendt (2008), Exhumation and deformation history of the lower crustal section of the Valstrona di Omegna in the Ivrea Zone, southern Alps, in *Tectonic Aspects of the Alpine-Dinaride-Carpathian System*, edited by S. Siegesmund, B. Fügeschuh, and N. Froitzheim, *Geol. Soc. London Spec. Publ.*, *298*, 45–68.

Smye, A. J., and D. F. Stockli (2014), Rutile U–Pb age depth profiling: A continuous record of lithospheric thermal evolution, *Earth Planet. Sci. Lett.*, *408*, 171–182, doi:10.1016/j.epsl.2014.10.013.

Spalla, M. I., and A. M. Marotta (2007), P-T evolutions vs. numerical modelling: A key to unravel the Paleozoic to early-Mesozoic tectonic evolution of the Alpine area, *Per. Mineral.*, *76*, 267–308.

Speranza, F., L. Minelli, A. Pignatelli, and M. Chiappini (2012), The Ionian Sea: The oldest in situ ocean fragment of the world?, *J. Geophys. Res.*, *117*, B12101, doi:10.1029/2012JB009475.

Sturani, C. (1964), Prima segnalazione di Ammoniti nel Lias del Canavese, *Rend. Accad. Lincei*, *37*, 482–483.

Torsvik, T. H., H. Amundsen, E. H. Hartz, F. Corfu, N. Kusznir, C. Gaina, P. V. Doubrovine, B. Steinberger, L. D. Ashwal, and B. Jamtveit (2013), A Precambrian microcontinent in the Indian Ocean, *Nat. Geosci.*, *6*, 223–227, doi:10.1038/NGEO1736.

Tugend, J., G. Manatschal, N. J. Kusznir, E. Masini, G. Mohn, and I. Thinon (2014), Formation and deformation of hyperextended rift systems: Insights from the mapping of the Bay of Biscay–Pyrenean rift system, *Tectonics*, *33*, 1239–1276, doi:10.1002/2014TC003529.

Turrini, C., O. Lacombe, and F. Roure (2014), Present-day 3D structural model of the Po Valley basin, Northern Italy, *Mar. Petrol. Geol.*, *56*, 266–289, doi:10.1016/j.marpetgeo.2014.02.006.

van Hinsbergen, D. J. J., M. Mensink, C. G. Langereis, M. Maffione, L. Spalluto, M. Tropeano, and L. Sabato (2014), Did Adria rotate relative to Africa?, *Solid Earth*, *5*, 611–629, doi:10.5194/se-5-611-2014.

Van Wijk, J. W., and S. A. P. L. Cloetingh (2002), Basin migration caused by slow lithospheric extension, *Earth Planet. Sci. Lett.*, *198*, 275–288.

Vance, J. (1999), Zircon fission track evidence for a Jurassic (Tethyan) thermal event in the Western Alps, *Mem. Sci. Geol. Padova*, *51*, 473–476.

Vavra, G., and U. Schaltegger (1999), Post-granulite facies monazite growth and rejuvenation during Permian to Lower Jurassic thermal and fluid events in the Ivrea Zone (Southern Alps), *Contrib. Mineral. Petrol.*, *134*, 405–414.

Vavra, G., R. Schmid, and D. Gebauer (1999), Internal morphology, habit and U–Th–Pb microanalysis of amphibolite-to-granulite facies zircons: Geochronology of the Ivrea Zone (Southern Alps), *Contrib. Mineral. Petrol.*, *134*, 380–404.

Velledits, F. (2006), Evolution of the Bükk Mountains (NE Hungary) during the Middle–Late Triassic asymmetric rifting of the Vardar-Meliata branch of the Neotethys Ocean, *Int J Earth Sci*, *95*, 395–412, doi:10.1007/s00531-005-0041-y.

Vermeesch, P. (2012), On the visualisation of detrital age distributions, *Chem. Geol.*, *312–313*, 190–194.

White, R. S. (1989), Initiation of the Iceland plume and opening of the North Atlantic, in *Extensional Tectonics and Stratigraphy of the North Atlantic Margins*, edited by A. J. Tankard and H. R. Balkwill, *Mem. Am. Assoc. Pet. Geol.*, *46*, 149–154.

Wolff, R., I. Dunkl, G. Kiesselbach, K. Wemmer, and S. Siegesmund (2012), Thermochronological constraints on the multiphase exhumation history of the Ivrea-Verbano Zone of the Southern Alps, *Tectonophysics*, *579*, 104–117, doi:10.1016/j.tecto.2012.03.019.

Zack, T., D. F. Stockli, G. L. Luvizotto, M. G. Barth, E. Belousova, M. R. Wolfe, and R. W. Hinton (2011), In situ U–Pb rutile dating by LA-ICP-MS: 208Pb correction and prospects for geological applications, *Contrib. Mineral. Petrol.*, *162*, 515–530.

Zanchetta, S., P. D'Adda, A. Zanchi, V. Barberini, and I. M. Villa (2011), Cretaceous-Eocene compressions in the central Southern Alps (N Italy) inferred from 40Ar/39Ar dating of pseudotachylytes along regional thrust faults, *J. Geodyn.*, *51*, 245–263, doi:10.1016/j.jog.2010.09.004.

Zanetti, A., M. Mazzucchelli, S. Sinigoi, T. Giovanardi, G. Peressini, and M. Fanning (2013), SHRIMP U–Pb zircon Triassic intrusion age of the Finero mafic complex (Ivrea–Verbano Zone, Western Alps) and its geodynamic implications, *J. Petrol.*, *54*, 2235–2265, doi:10.1093/petrology/egt046.

Zezza, U., S. Meloni, and M. Oddone (1984), Rare earth and large-ion-lithophile element fractionation in late Hercynian granite massif of the Biellese Area (Southern Alps, Italy), *Rend. Soc. Ital. Mineral. Petrol.*, *39*, 509–521.

Zingg, A., J. C. Hunziker, M. Frey, and H. Ahrendt (1976), Age and degree of metamorphism of the Canavese Zone and of the sedimentary cover of the Sesia Zone, *Schweiz. Mineral. Petrogr. Mitt.*, *56*, 361–365.